



**JOINT  
RESEARCH  
CENTRE**

**ANNUAL PROGRESS REPORT ON NUCLEAR DATA  
1996**

**INSTITUTE FOR REFERENCE MATERIALS AND MEASUREMENTS  
GEEL (BELGIUM)**





**JOINT  
RESEARCH  
CENTRE**

**ANNUAL PROGRESS REPORT ON NUCLEAR DATA  
1996**

**INSTITUTE FOR REFERENCE MATERIALS AND MEASUREMENTS  
GEEL (BELGIUM)**

## **LEGAL NOTICE**

**Neither the Commission of the European Communities nor any person acting on behalf of the Commission is responsible for the use which might be made of the following information**

# TABLE OF CONTENTS

	Page
<b>EXECUTIVE SUMMARY</b> .....	1
<b>NUCLEAR DATA</b> .....	3
NUCLEAR DATA FOR STANDARDS .....	4
NUCLEAR DATA FOR FISSION TECHNOLOGY .....	19
Neutron Data of Actinides .....	19
Neutron Data of Structural Materials.....	25
SPECIAL STUDIES .....	29
NUCLEAR DATA FOR FUSION TECHNOLOGY.....	41
<b>NUCLEAR METROLOGY</b> .....	45
RADIONUCLIDE METROLOGY .....	45
<b>TECHNICAL APPENDIX</b> .....	57
<b>LIST OF PUBLICATIONS</b> .....	66
<b>GLOSSARY</b> .....	70
<b>CINDA ENTRIES LIST</b> .....	72

Note: For further information concerning the Project Nuclear Measurements (Nuclear Data, Nuclear Metrology), please contact A.J. Deruytter, Project Manager, IRMM, Retieseweg, B-2440 Geel, Belgium.

Editor: H.H. Hansen

## *Executive Summary*

A.J. Deruytter

In 1996, The second year of the Fourth Framework Programme, the main objectives of the project "Reference Measurements" have been pursued in the sub-projects "Nuclear Data" and "Nuclear Metrology": (1) to improve the neutron standards data set, relative to which partial cross-sections or other quantities, important for fission and fusion technology are determined; (2) to improve the knowledge of radionuclide decay data for standards applications; (3) to develop nuclear measurement techniques for nuclear and non-nuclear applications.

The IRMM continued to use the two strong neutron sources of the Institute (GELINA and the 7 MV Van de Graaff) for neutron data measurements for applied purposes. The detailed programme follows the recommendations of the OECD-NEA Nuclear Science Committee and in particular its Working Party on International Evaluation Co-operation. These activities are co-ordinated by IRMM in the frame of the NEA Working Party on Experimental Activities. Major activities were the measurement of neutron total and capture cross-sections for  $^{99}\text{Tc}$  and  $^{237}\text{Np}$  in the resonance region, needed for waste transmutation studies, in close collaboration with CEA, Saclay (F), and an investigation of the Doppler broadening of neutron resonances, important for the calculation of the temperature coefficient of reactivity of reactors, an important safety parameter in a network with as prominent partners CEA, Cadarache (F) and ILL, Grenoble (F). Also, high resolution measurements of the inelastic scattering cross-section of iron, important for shielding calculations, have been performed using a 200 m flight-path. The cross-sections for inelastic scattering from low-lying levels of Molybdenum isotopes, weakly absorbing fission products, were measured in response to a long standing request for the JEF project. Accurate measurements and data analysis were performed to improve the set of nuclear measurement standards, in particular for the total cross-section of  $^{10}\text{B}$ , and the fission fragment mass yield and kinetic energy distributions and fission neutron spectra of  $^{252}\text{Cf}$ .

In radionuclide metrology solutions of  $^{63}\text{Ni}$  and  $^{55}\text{Fe}$  were standardised by liquid scintillation in the frame of a EUROMET comparison, and under the aegis of the BIPM, IRMM participated in a comparison by activity measurements of a solution of  $^{192}\text{U}$ . Low

energy X-ray sources were prepared, standardised and sold. A bone ash reference material was successfully characterised for radioactivity in an international collaboration.

At the Linac, a dedicated laboratory is being completed to develop applications in the field of radiation physics and at the 7 MV Van de Graaff nuclear reaction and backscattering techniques were applied to analyse hydrogenated B-C-N thin films deposited on Si substrates in the frame of FUNINCOAT, a network for the development and characterisation of super hard coatings.

## NUCLEAR DATA

### *Nuclear Energy Agency Nuclear Science Committee Working Party for Measurement Activities (WPMA) : Mission and Status Report*

H. Weigmann, E. Wattecamps, A. Deruytter, D.L. Smith\*, C. Nordborg\*\*

The Working Party on International Nuclear Data Measurements Activities (WPMA) was organised in 1994 under the auspices of the Nuclear Energy Agency Nuclear Science Committee, to serve as an independent standing committee with equal status to the already existing Working Party on International Evaluation Co-operation (WPEC). This was done in recognition of the importance of experimental activities and experimental data to the overall process of generating reliable nuclear data for applications. The first meeting of the WPMA took place at Oak Ridge National Laboratory in May 1994, just prior to the 1994 Gatlinburg Nuclear Data Conference. There have been three other meetings (on an annual basis) since then. The WPMA is comprised of representatives from laboratories in the U.S., Europe, Japan and the Former Soviet Republics. The major objective is to ensure an efficient use of the limited experimental resources left world-wide in the area of neutron data measurements. To this end the group 1) encourages measurements to be carried out at appropriate equipped laboratories in support of the NEA evaluation efforts, 2) encourages collaborations that effectively match available personnel and facilities 3) edits, on an approximately annual basis, a "Newsletter on International Nuclear Data Measurement Activities" for a systematic and complete communication between experimental laboratories and groups active in nuclear data evaluation. This paper will discuss the on-going activities of the WPMA and will describe its most significant achievements to date.

### *Update of the NEANSC/INDC Nuclear Standards Report, <sup>10</sup>B*

F.-J. Hamsch, A. D. Carlson\*\*\*

An IAEA Consultants Group has examined the neutron cross section database for possible new standards and extensions in energy of existing standards. This effort has led to an update of the 1991 NEANDC/INDC Nuclear Standards Report<sup>(1)</sup> to indicate the status and

---

\* Argonne National Laboratory, Argonne, USA

\*\* NEA, Paris, France

\*\*\* National Institute of Standards and Technology (NIST) Gaithersburg, USA

(1) Technical Report Series, Nuclear Data Standards for Nuclear Measurements, NEANDC - 311 U, INDC(SEC)-101, 1992

extension of cross section standards for the  $^{10}\text{B}(n,\alpha)$  reaction in the energy region below 20 MeV, the  $\text{H}(n,n)$  and the fission cross sections for  $^{235}\text{U}$ ,  $^{238}\text{U}$  and Bi for the energy range 20-350 MeV. The work on the  $^{10}\text{B}(n, \alpha)$  reaction was motivated by the need to improve the database for this standard which has many discrepant data sets and to extend the energy range over which it can be used as a standard. For the other reactions new data have been measured which motivated a renewed review of these cross sections. The objective of this work is to provide concise and readily useable reference guidelines for essential nuclear standards quantities for a variety of basic and applied endeavours.

## NUCLEAR DATA FOR STANDARDS

The objective of the work on standard nuclear data is to improve the set of neutron data to be used in measurements consistency checks. Competing reactions, angular and kinetic energy distributions of the reaction products have to be studied to increase the reliability of the given standard cross sections. Appropriate research topics are selected from listings of the INDC:NEANDC Standards file. Complementary work is devoted to radionuclide decay data and associated atomic data requested for calibration and reference purposes.

### *Analysis of the prompt fission neutron spectrum of $^{252}\text{Cf}$*

N. Kornilov\*, F.-J. Hambsch

The experimental data on the prompt fission neutron spectra (PFNS) of Budtz-Jørgensen and Knitter<sup>(2)</sup> have been re-analysed with a new method, based on the analysis of neutron energy-angular distributions in the laboratory system (LS). This new approach did not need any "a priori" information on the spectrum shape.

The PFNS in the LS are usually estimated on the basis of the assumption that the neutrons are emitted by fully accelerated fragments. Therefore, the center-of-mass system (CMS) velocity may be calculated on the basis of fragments masses and their total kinetic energies (TKE). Hence, the knowledge of the CMS angular distribution and spectrum parameters depends on the validity of this assumption.

---

\* Visiting Scientist from Institute of Physics and Power Engineering, Obninsk, Russia  
 (2) C.Budtz-Jørgensen, H.-H.Knitter, Nuclear Physics, A490, (1988), 307

Some evidence is given<sup>(1)</sup> that the fragment kinetic energy at the moment of neutron emission is less than TKE. This conclusion was drawn on the basis of the analysis of angular integrated spectra in the LS. However, this indirect method may introduce distorting effects and result in a wrong conclusion. Therefore, a new method, the CMS velocity estimation method, based on the analysis of neutron energy-angular distributions in the LS was developed<sup>(2)</sup>. Both the original data set<sup>(2)</sup> and the re-analysed one show that there are low energy neutrons with a particular angular distribution. These neutrons can not be described in the model of neutron emission from a moving source. Therefore, only the neutron energy range from 2 to 7 MeV was used to analyse the experimental data and fitted with the new method. The fitted parameters are collected in Table 1.

The lower fragment kinetic energy means, that neutrons may be emitted during all the time interval from scission to total relaxation before the fragments reach full acceleration. An example of the experimental data and the fitted curves are shown in Fig. 1. It is obvious that the experimental data can not be described by the model of neutron emission by fully accelerated fragments (dashed line).

The CMS spectra for both fragments are shown in Figs.2;3. The spectra can not be described by the formula:

$$S(\varepsilon) = \frac{\varepsilon^\lambda}{\Gamma(\lambda+1)T^{\lambda+1}} \exp\left(-\frac{\varepsilon}{T}\right) \quad (1)$$

Only the sum of two spectra  $S(\varepsilon)=S_1(\varepsilon)+S_2(\varepsilon)$  gave a reasonable agreement with the experimental results. The parameters for the CMS spectra are given in Table 2. The average energies estimated by the integration of the experimental data points are:  $\langle\varepsilon_l\rangle=1.560$  MeV,  $\langle\varepsilon_h\rangle=1.431$  MeV and they agree quite well with the data estimated by the relation:

$$\langle\varepsilon\rangle=(\lambda_1+1)T_1*Y_1+(\lambda_2+1)*T_2*Y_2,$$

where  $Y_i$  is the neutron yield for each spectra. The absolute neutron yield was normalised to  $v = 3.766$ .

The surplus neutron spectrum, visible in Fig. 1, which has a particular angular distribution and rather high yield (4.5 %), was calculated as a difference between the experimental data and the fitted curve and is shown in Fig. 4. The experimental points were fitted by eq. (1) and the parameters are given in the last row of Table 2.

<sup>(1)</sup> N.V.Kornilov, A.B. Kagalenko, Proc. of XII Meeting on Phys. of Nuclear Fission, Obninsk, 1993, Journal of Nucl. Phys. 57 (1994) 1172.

<sup>(2)</sup> N.V. Kornilov, A.B.Kagalenko, ISINN-3, Dubna 1995, p. 213

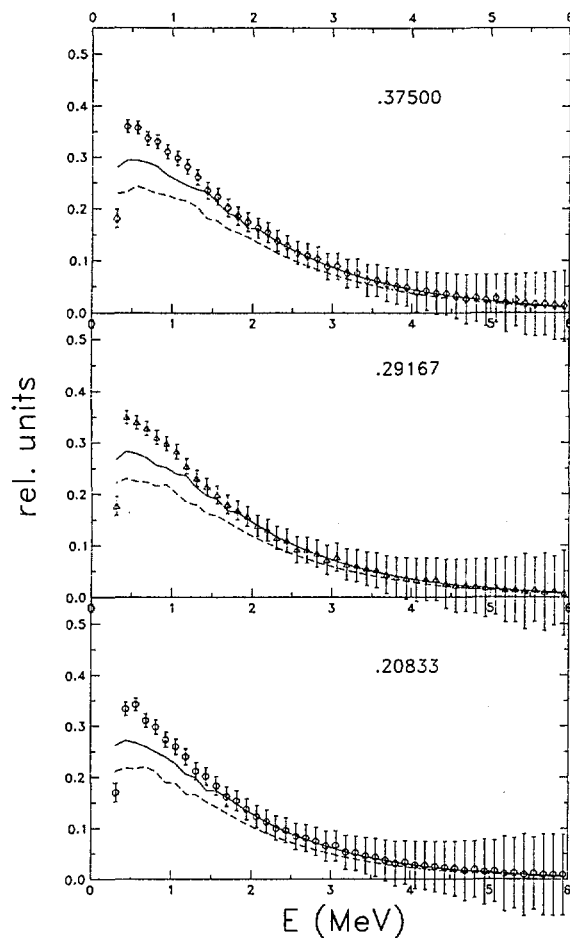


**Fig. 1.** Neutron spectra versus energy for different angles in the LS. The number corresponds to the cosine-values. The symbols represent the experimental data. The full line is the calculated spectra with the fitted parameters (Table 1, column 3). The dashed line is the spectra with fixed parameters (Table 1, column 5)

**Table 1.** The CMS parameters estimated in this work. B-data represent the original data set. H-data is the re-evaluated data set.  $\alpha = E_v(B,H)/E_v(\text{full})$ , with  $E_v$  the fragment kinetic energy per nucleon and  $b$  the anisotropy parameter

	param.	B-data	H-data	Full acc.
LF	$E_v, \text{MeV}$	$0.865 \pm 0.002$	$0.844 \pm 0.002$	0.958
	$\alpha$	$0.902 \pm 0.002$	$0.881 \pm 0.002$	1.0
	$b$	$0.018 \pm 0.003$	0.0	0.0
HF	$E_v, \text{MeV}$	$0.479 \pm 0.002$	$0.489 \pm 0.002$	0.557
	$\alpha$	$0.860 \pm 0.003$	$0.877 \pm 0.004$	1.0
	$b$	$0.011 \pm 0.003$	0.0	0.0

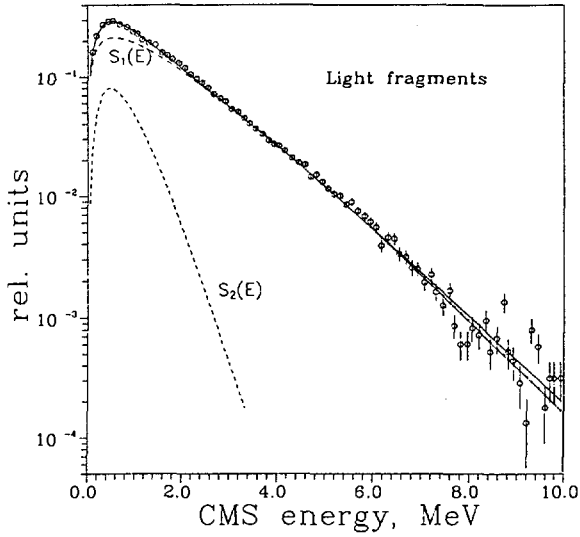


**Fig. 2.** Spectrum of neutrons for the light fragments in the CMS. Circles are the experimental data. Dashed lines show the partial spectra (see text). Solid line shows the total spectrum. Solid line with dots presents the spectra with  $T_2=0.97*T_1$  for the energy range above 6 MeV

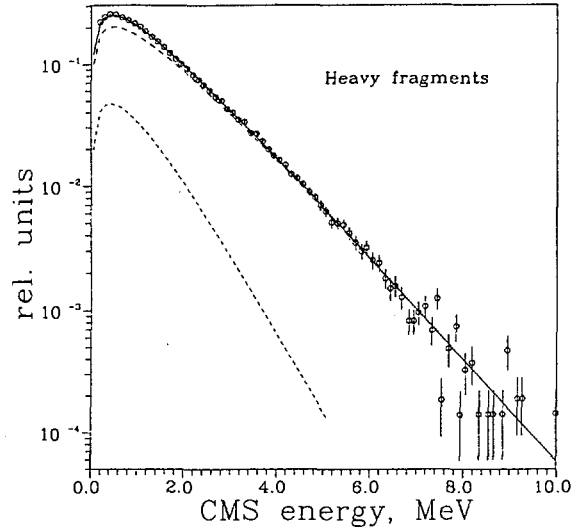


**Fig. 3.** CMS spectrum of neutrons for the heavy fragments.  $S_1(E)$ ,  $S_2(E)$  and total spectra are shown by lines

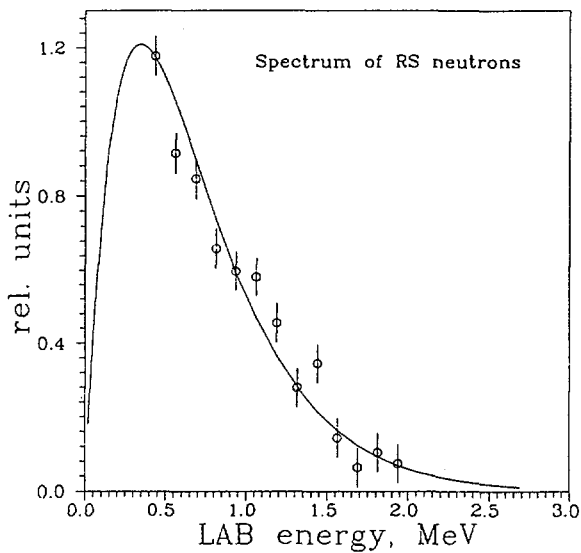


**Fig. 4.** Spectrum of the surplus neutrons. The solid line represents a Maxwell distribution with  $t=0.346$  MeV

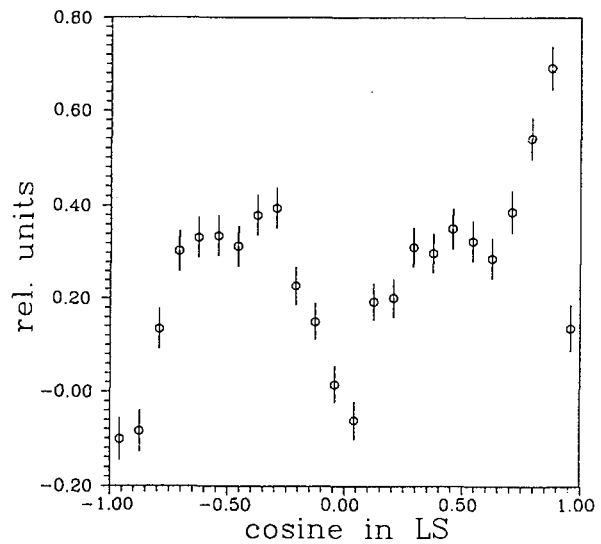


**Fig. 5.** Angular distribution of the surplus neutrons

**Table 2. Parameters for the CMS neutron spectra.  $\nu$  is the number of prompt neutrons**

	$\lambda$	T, MeV	$\nu$	$\langle \epsilon \rangle$	Y
LF, S1( $\epsilon$ )	0.5	1.115	1.698	1.673	0.451
S2( $\epsilon$ )	1.6	0.308	0.283	0.802	0.075
HF, S1( $\epsilon$ )	0.5	0.984	1.398	1.477	0.371
S2( $\epsilon$ )	0.7	0.609	0.220	1.036	0.058
RSN, S(E)	1.0	0.346	0.168	0.692	0.045

The angular distribution of the surplus neutrons has a rather unusual shape (see Fig. 5). The average energy of the neutron spectra in the LS when all neutron sources are included is 2.127 MeV. This value is in good agreement with the evaluation of Mannhart<sup>(1)</sup>  $\langle E \rangle = 2.121$  MeV. Leaving, however, the surplus neutrons out, the average energy is 2.194 MeV. It seems that the spectrum calculated with the fitted parameters shows a better agreement than the one calculated under the assumption of emission from fully accelerated fragments.

No correction was applied up to now for neutron multiple scattering (MS) in the ionisation chamber. The scattered neutrons should have an isotropic angular distribution. However, the relative contribution of MS neutrons may depend on the neutron emission angle. The MS correction is presently being estimated. The final conclusion concerning the above mentioned findings will be made only after this additional data correction.

### ***Investigation of the Far Asymmetric Region in $^{252}\text{Cf}(SF)$***

F.-J. Hamsch, S. Oberstedt\*

Extensive effort has been devoted to study fission fragment mass and energy distributions in low energy fission<sup>(2)</sup>. By radiochemical methods mass yields have been measured down to and below the  $10^{-4}$  % yield level. No deviation from the smooth decrease of the yield in the far asymmetric mass region was observed.

(1) W. Mannhart, Proc. of IAEA Group Meet. on Neutron Source Prop., Leningrad 1986, (Ed. K. Okamoto), IAEA-TECDOC-410 (1987), 158

\* EC Fellow from the TH Darmstadt, Germany

(2) F. Gönnerwein; The Nuclear Fission Process, C. Wagemans (editor), CRC Press Inc., Boca Raton, Florida, 1991, page 287 ff

More than a decade ago, however, first evidence has been reported<sup>(1,2)</sup> for an enhanced far asymmetric yield in the spontaneous fission of  $^{252}\text{Cf}$ . Also radiochemical investigations of the far asymmetric mass range for the fission of  $^{238}\text{U}$  showed<sup>(3,4)</sup> an enhanced yield for masses larger (smaller) than 160 (80), but the yield level is two orders of magnitude lower in  $^{238}\text{U}$  than in  $^{252}\text{Cf}$ . Most recently a measurement of Goverdovsky et al<sup>(5)</sup> for  $^{236}\text{U}(n,f)$  at  $E_n = 1$  MeV revealed a far asymmetric yield level of higher than  $10^{-3}$  % with exhibition of a two peak structure at  $A \sim 64$  and  $70$  amu. The observed structure was associated with a new valley in the potential energy landscape leading to the  $Z = 28$  magic proton shell closure. The production of neutron rich nuclei close to the doubly magic shell closure  $Z = 28$ ,  $N = 50$  is also the main reason of the recent attention on the far asymmetric mass region. The fission process could be considered as a production source of these neutron rich nuclei and spontaneous fission is especially interesting, since no beam time is needed. However, the interpretation of results should be made very careful because it depends very much on the target quality and geometry used.

A twin Frisch-gridded ionisation chamber has been used to measure the fission fragment mass, kinetic-energy and angular correlations for  $^{252}\text{Cf}(\text{SF})$ . In total  $2.5 \cdot 10^8$  events were collected. The californium source was prepared by vacuum evaporation on a  $120 \mu\text{g}/\text{cm}^2$  nickel backing with a source strength of about 1500 fission/s at the time of the measurement. With the angle information at hand the angular dependent energy-loss in the source and backing was corrected. The angle information made also possible to select fission fragments as a function of the angular cone, which was crucial in determining the far asymmetric events. The resulting pre-neutron mass distribution is shown in logarithmic scale in the upper part of Fig. 6, together with the mean total kinetic energy (TKE) (middle part of Fig. 6) and the square root of the variance as a function of the fragment mass (lower part of Fig. 6). Only those events have been taken into account in the analysis, where the  $\cos\theta$  was larger than 0.5. The dotted line should guide the eye and results from a Gaussian fit to the asymmetric mass distribution. As it is obvious the enhanced yield at far asymmetric fission as observed earlier<sup>(3)</sup> for  $^{252}\text{Cf}$  is confirmed.

---

<sup>(1,2)</sup> M. Asghar, F. Caitucoli, P. Perrin, T.P. Doan, G. Barreau and B. Leroux, Nucl. Phys. A341 (1980) 388.

G. Barreau, A. Sicre, F. Caitucoli, M. Asghar, T.P. Doan, B. Leroux, G. Martinez and T. Benfoughal, Nucl. Phys. A432 (1985) 411.

<sup>(3,4)</sup> V.K. Rao, V.K. Bhargava, S.G. Marathe, S.M. Sahakundu and R.H. Iyer, Phys. Rev. C19 (1979) 1372. D.R. Nethaway, B. Mendoza and T.E. Voss, Phys. Rev. 182 (1969) 1251.

<sup>(5)</sup> A.A. Goverdovsky, V.F. Mitrofanov and V.A. Khryachkov, Phys. At. Nucl. 58 (1995) 1460.

However, due to the much higher statistical accuracy the fluctuations in TKE and  $\sigma_{\text{TKE}}$  are now significantly reduced and the effect seems to be more pronounced. The mass range is now extended to well beyond  $A_L/A_H = 72/180$ . However, due to the better statistics in the present work, it is also possible to reduce the cone in  $\cos\theta$  in the off-line analysis to only those events where  $\cos\theta$  is larger than 0.9. The result is shown in Fig. 7. Still the total number of events is  $2.4 \cdot 10^7$ . However, the distributions shown in Fig. 7 look very different to the ones of Fig. 6, if only the far asymmetric region is concerned. There is no enhanced yield visible any longer above (below) mass  $A_H = 176$  ( $A_L = 76$ ) and the yield dependence follows nicely the dotted line down to the yield level of  $10^{-5}$  %. The mean TKE also continues to drop. Finally, also the  $\sigma_{\text{TKE}}$  does not show any additional increase, which could suggest the onset of a new different mode. There is a slight increase visible at around  $A_L/A_H = 86/166$  with still very good statistical accuracy, but this is already visible in Fig. 6 and seems therefore to be real and is also reflected as a shoulder in the TKE distribution.

New calculations in the frame of the multi-modal random neck-rupture model of Brosa et al.<sup>(1)</sup> have shown that the so-called super-asymmetric fission mode is expected in the mass range around  $A \sim 160$ . But with a very high and broad additional barrier, the expected yield should be actually negligible.

Hence, it has been shown that one should be cautious in interpreting results in very low mass yield regions, where the resolution is very much dependent on the quality of the whole experimental set-up.

### ***The Multi-modal Random Neck-Rupture Model: Revision and Application***

S. Oberstedt\*, F.-J. Hambsch, F. Vivès\*\*

Calculations in the frame of the multi-modal random neck-rupture model have been performed for  $^{239}\text{U}$ . For the first time the identification of fission modes has been based on reproducible selection criteria, because the determination of a particular fission mode has tended in the past to follow pattern which are biased by experimental results.

---

<sup>(1)</sup> U. Brosa, S. Großmann and A. Müller Physics Reports 197 (1990) 167.

\* EC Fellow from the TH Darmstadt, Germany

\*\* EC Fellow from the University of Bordeaux, France

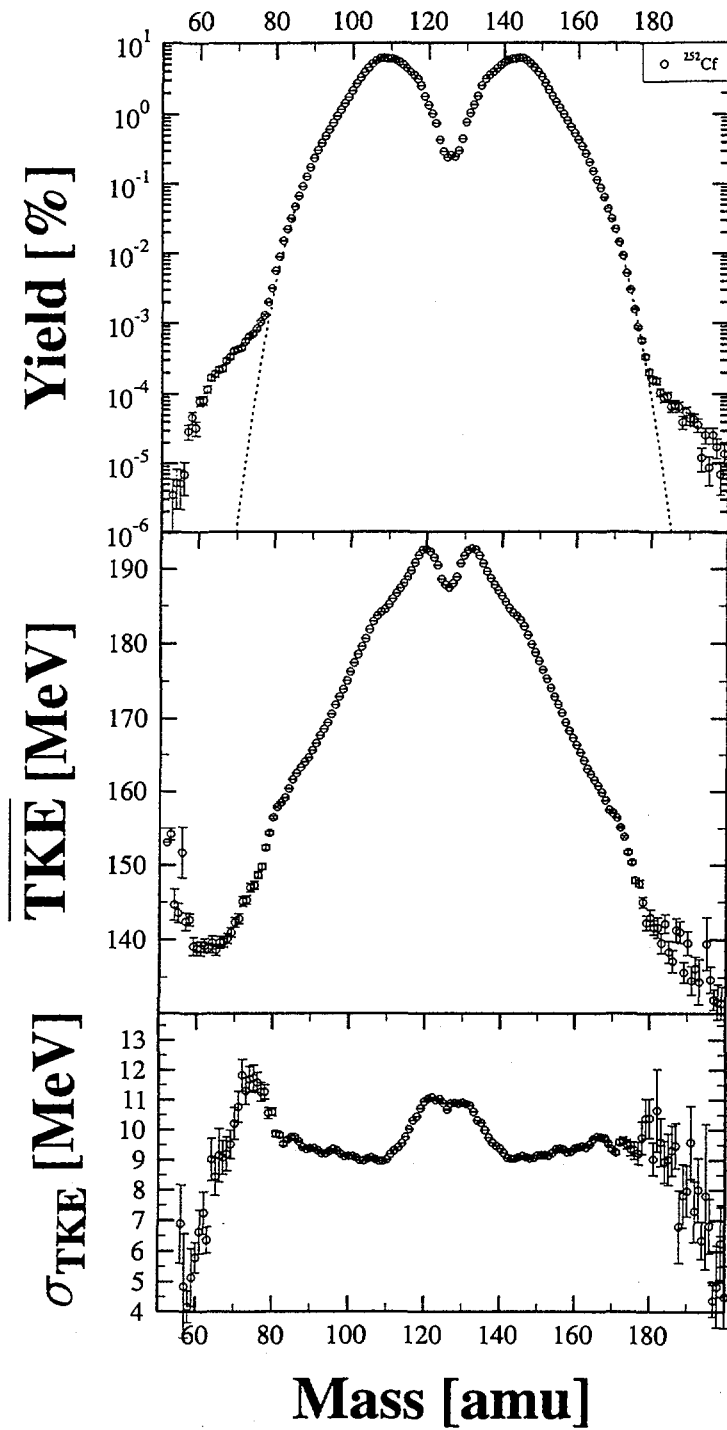


Fig. 6. Pre-neutron distributions. Upper part: the mass-yield in logarithmic scale; middle part: the mean total kinetic energy (TKE); lower part: the square root of the variance of the total kinetic energy distributions, plotted versus the fragment mass. The events are selected for  $\cos\theta > 0.5$ . The dotted line shows the estimated yield dependence deduced from a Gaussian fit to the asymmetric mass yield

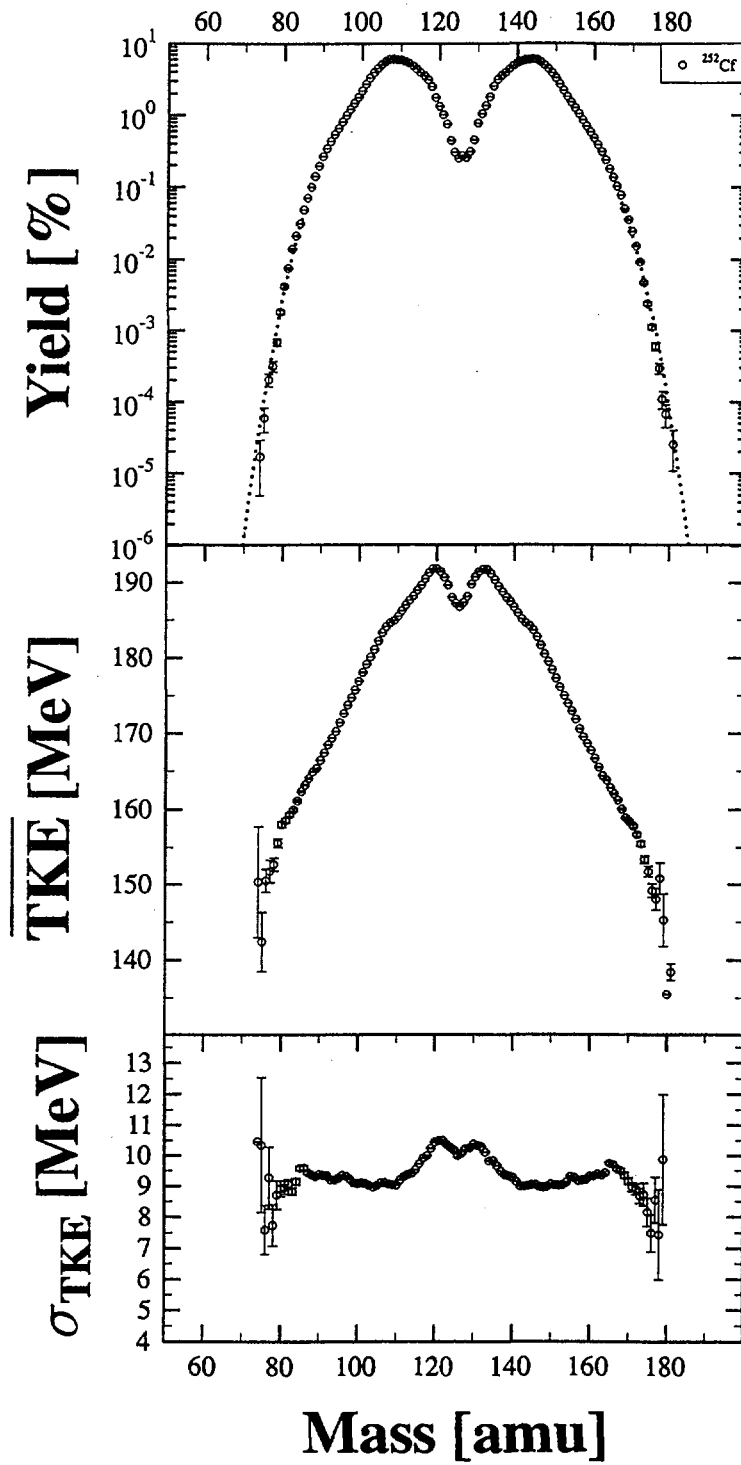
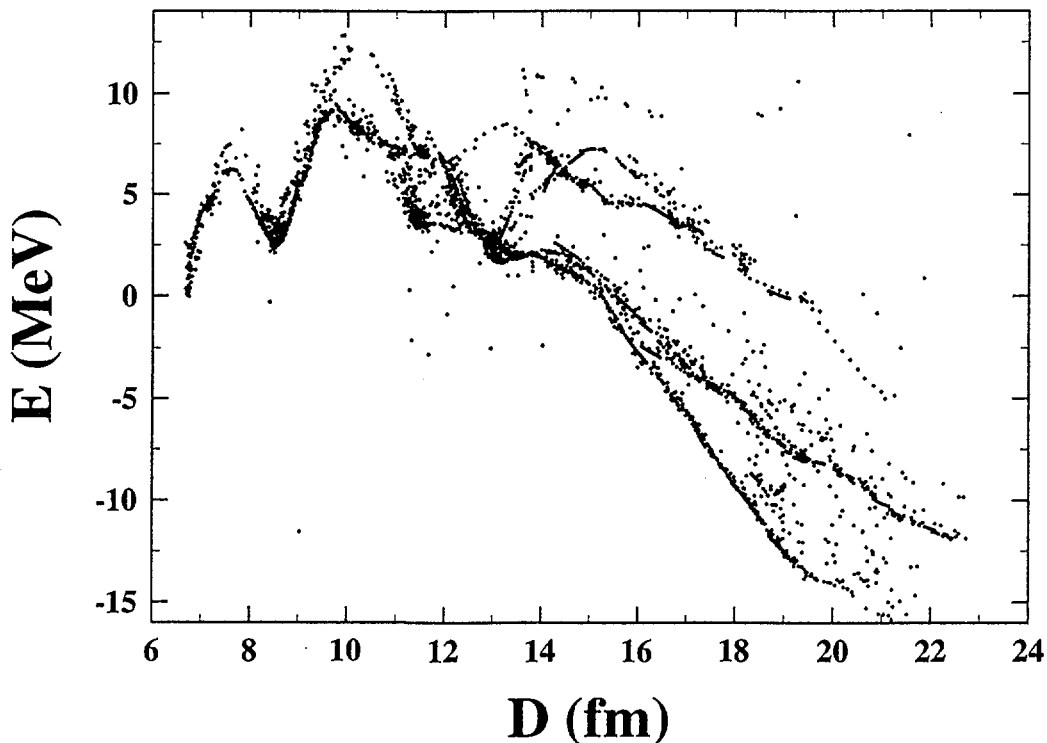


Fig. 7. Same as Fig. 6, but for selecting events with  $\cos\theta > 0.9$

In total 3300 minimised shape configurations have been calculated. The calculated energy  $E$  is shown in Fig. 8 as a function of  $D$ , the distance of the future fragments. The overall shape of the existing fission modes as well as the characteristic double-humped fission barrier are visible. In order to identify each particular fission mode, the data are sorted in ascending order in  $D$  and roughly according to their asymmetry  $z$ .

The following criteria have been applied to the data of each apparent fission mode :

- For increasing  $D$  the neck radius  $r$  has to decrease gradually,
- At the same time, the semi-length  $l$  of the nuclear shape should increase,
- Fluctuations in the respective mass-split, taken for the heavy fragment, should be smaller than a certain maximum value,
- In all steps the change in potential energy should be smooth,
- The centre-of-mass parameter  $s$  must have the opposite sign of the corresponding asymmetry parameter  $z$ , i. e.  $s*z < 0$ , and



*Fig. 8. Overview of all calculated minimised points in the potential energy landscape of  $^{239}\text{U}$ . The gross shape of the existing fission modes as well as the double-humped fission barrier are visible*

- For increasing  $D$  the curvature parameter  $c$  has to increase.

Points which do not fulfil all the conditions have to be rejected as spurious. The thus selected shape configurations are shown in Fig. 9 as projections on the most illustrative two-dimensional subspaces, namely  $E(D)$  and  $A_h(D)$ . As indicated by the inserts, six fission modes theoretically exist in  $^{239}\text{U}$ . The labelling is preliminary and partially according to already existing labels<sup>(1)</sup>. The most striking result is, that all physically relevant fission modes branch off in the shape isomeric ground state, thus exhibiting different outer barriers. In additions the mean mass-splits known from experimental mass-distributions have been identified. Unfortunately, for  $^{239}\text{U}$  the experimentally observed mass-split at about  $A_h = 135$  could not be verified. The scission point of each fission mode is investigated by applying the Rayleigh criterion  $l \geq 11/2r$  to the calculated data. For each of these points the total kinetic energy TKE is calculated from the distance of the centre of charges of both fragments, which is in fact  $D$  from the fission mode calculations since a constant charge distribution is always assumed. The obtained results are shown in Fig. 10 and numerical values are given in Table 3. From this figure the following conclusions may be drawn :

- Scission is possible along a certain range of shape configurations,
- These manifold scission configurations existing for each fission mode result directly in a rectangular distribution of possible TKE values, which have an equivalent Gaussian width compatible with typical experimental results,
- A non-negligible spread of the characteristic mean mass-split should be noticed, and
- The calculated mean masses as well as the mean TKE values and the corresponding widths  $\sigma_{\text{TKE}}$  of the established modes are in the expected range.

**Table 3. Characteristic parameters obtained from fission mode calculations for  $^{239}\text{U}$**

Fission mode	$A_h$ (amu)	$\sigma_A$ (amu)	$Z_h$	TKE (MeV)	$\sigma_{\text{TKE}}$ (MeV)
std	137.1	0.26	52.8	177	6
012	139.1	0.22	53.5	176	6
011	141.9	0.34	54.6	165	8
s3	154.2	0.24	59.4	171	1
sl	119.8	0.08	46.1	159	7
s5	136.4	0.14	52.5	157	2

<sup>(1)</sup> U. Brosa, S. Großmann and A. Müller, Phys. Rep. 197 (1990) 167

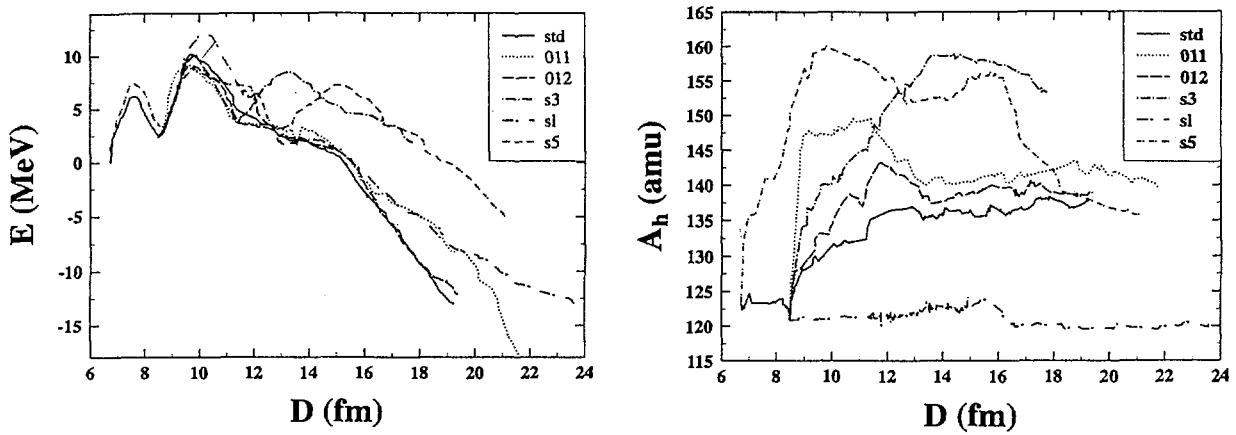


Fig. 9 Fission modes in  $^{239}\text{U}$  extracted by the selection criteria mentioned in the text. The most striking result is that all modes, except the one labelled (s5), branch off in the shape isomeric minimum

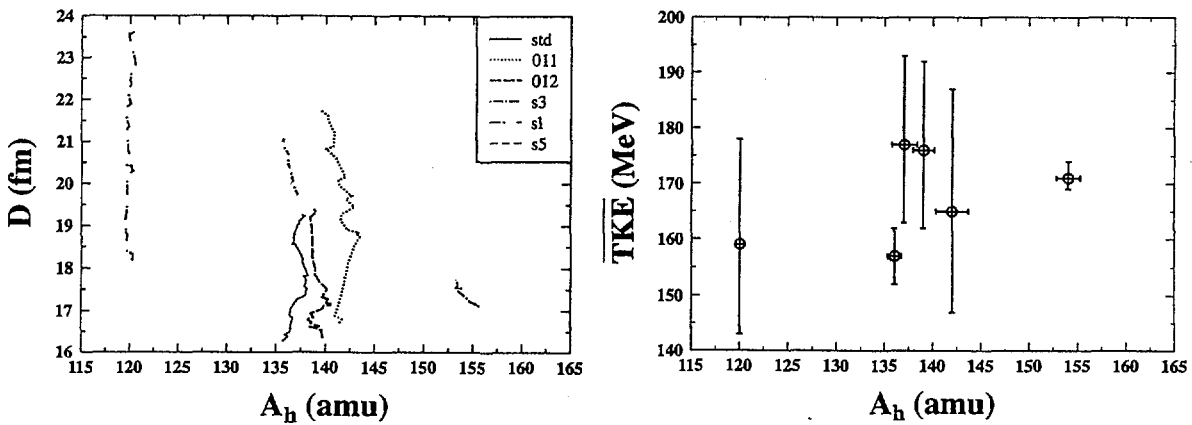


Fig. 10. Left part : All shape configurations for which the Rayleigh criterion is fulfilled displayed as the distance of the forming fragments  $D$  as a function of the corresponding mass-split expressed by the heavy fragment mass  $A_h$ . Right part: Corresponding TKE as a function of  $A_h$

## *Investigation of the $^{238}\text{U}(n,f)$ -Process at Incident Neutron Energies Between 1.6 and 3.5 MeV*

F. Vivès\*, F.-J. Hamsch, H. Bax

Even though  $^{238}\text{U}$  is one of the major standards, the data available concerning the fission fragment properties and their dependence on incident neutron energy are rather scarce. Therefore a new investigation of the  $^{238}\text{U}(n,f)$ -process has been started in the present reporting period. The 7 MV-Van de Graaff accelerator has been used to deliver the neutrons via the  $\text{T}(p,n)^3\text{He}$  reaction in the energy range from 1.6 MeV to 3.5 MeV. With a Frisch girded ionisation chamber the fission fragment mass, kinetic energy and angular distributions have been measured.

In parallel, theoretical calculations based on the multi-modal random neck-rupture model of Brosa et al.<sup>(1)</sup> have been accomplished and will be used for comparison to the experimental results.

The raw data have been corrected event wise for the inefficiency of the Frisch grids, the pulse-height defect in the counter gas and the energy loss in the fissioning target.

For the pre-neutron mass determination the shape of the sawtooth  $v(A)$  of the  $^{238}\text{U}$  has been deduced from the already known ones of  $^{233}\text{U}$  and  $^{235}\text{U}$  and is shown in Fig. 11. The absolute energy calibration was based on the thermal neutron induced fission of  $^{235}\text{U}$ . The comparison of the resulting mass distribution with the one of the  $^{235}\text{U}(n_{\text{thermal}},f)$  is shown in Fig. 12. The shift in the mass distribution shows similarities to those observed in the case of several spontaneously fissioning plutonium-isotopes<sup>(2)</sup>. The preliminary values of TKE as a function of  $E_n$  for the reaction  $^{238}\text{U}(n,f)$  are given in Table 4 below.

**Table 4.** *Preliminary TKE values as a function of  $E_n$  obtained using the  $^{238}\text{U}$  sawtooth, or the already known one of  $^{239}\text{Pu}$*

$E_n$ [MeV]	( $^{238}\text{U}$ sawtooth)	( $^{239}\text{Pu}$ sawtooth)
1.6	$170.31 \pm 0.04$	$170.32 \pm 0.04$
1.7	$170.31 \pm 0.04$	$170.32 \pm 0.04$
1.8	$170.36 \pm 0.03$	$170.36 \pm 0.03$
2.0	$170.37 \pm 0.03$	$170.39 \pm 0.03$
2.5	$170.36 \pm 0.03$	$170.36 \pm 0.03$
3.0	$170.33 \pm 0.03$	$170.34 \pm 0.03$
3.5	$170.11 \pm 0.03$	$170.12 \pm 0.03$

\* EC Fellow from the University of Bordeaux, France

<sup>(1)</sup> U. Brosa, S. Großmann and A. Müller, Phys. Rep. 197 (1990) 167

<sup>(2)</sup> L. Dematte et al., Proc. Seminar on fission "Pont d'Oye III", ed. C. Wagemans, EUR 16295, p.66

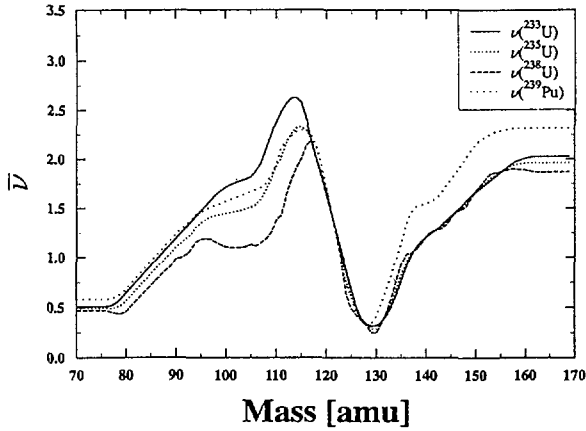


Fig. 11. The sawtooth of 3 isotopes of Uranium and of  $^{239}\text{Pu}$ , the one of  $^{238}\text{U}$  has been deduced from the known ones of  $^{233}\text{U}$  and  $^{235}\text{U}$

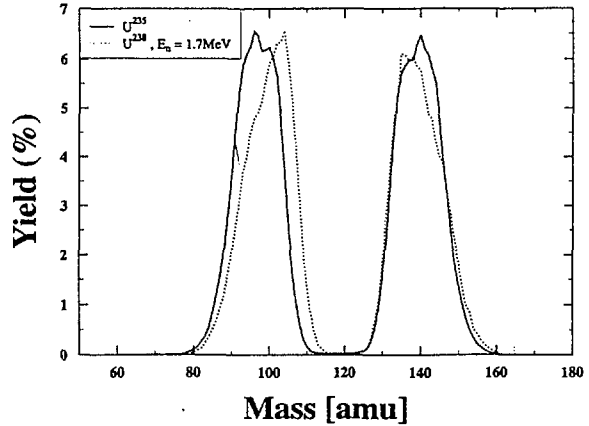


Fig. 12. Comparison of the mass yield of  $^{235}\text{U}(n_{\text{thermal}},f)$  and  $^{238}\text{U}(n,f)$  at  $E_n=1.7\text{MeV}$

Compared to the results of Vorob'eva et al.<sup>(1)</sup> the absolute value of TKE and its dependence on  $E_n$  are not the same, which seems mainly due to the fact that they have used the sawtooth of  $^{239}\text{Pu}$  ( $E_n = \text{thermal}$ ) with a constant  $v_t(E_n) = v_{\text{Thermal}}(^{239}\text{Pu})$  for each of the investigated energies in the pre-neutron mass calculation. The comparison of both results is presented in Fig. 13 where the symbols ( $\diamond$ ) represent the values of TKE obtained from the present data when using  $v_{\text{Thermal}}(^{239}\text{Pu})$ .

The TKE shows a smooth behaviour as a function of  $E_n$  over the neutron energy range studied, with an apparent drop at the highest value of  $E_n$ , which is partly due to a change in the mass yield distribution. This result does not depend on whether the prompt  $v(A)$  correction to the fragment masses is based on the shape of  $v(A)$  of  $^{239}\text{Pu}$  or on the one of  $v(A)$  of  $^{238}\text{U}$  estimated previously. The difference in the TKE(A) distribution between  $E_n = 2\text{ MeV}$  and  $E_n = 3.5\text{ MeV}$  is presented in Fig. 14. An apparent slope is noticeable, since besides mass yield variations also changes in TKE(A) are responsible for the decrease of TKE at the highest value of  $E_n$ .

The angular distribution has been analysed too. In order to exclude resolution effects, only the range  $0.2 \leq \cos\theta \leq 0.9$  has been fitted by Legendre polynomials. The deduced anisotropy coefficient  $A = W(0)/W(90) - 1$  is compared to existing data<sup>(2)</sup>. The agreement

(1) V.G. Vorob'eva et al., Sov. J. Nucl. Phys. 50 (1989) 574

(2) D.L. Shpak, Sov. J. Nucl. Phys. 50 (1989) 574

is rather good, even though not much improvement could be reached including the 4<sup>th</sup> order term in the Legendre polynomials as was the case for Shpak<sup>(1)</sup>

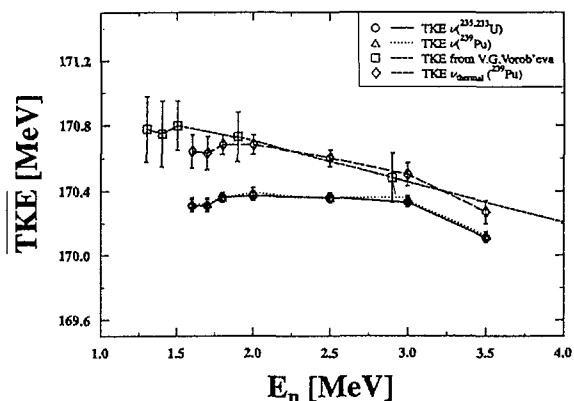


Fig. 13. Preliminary TKE values as a function of  $E_n$  (O,  $\diamond$ ) compared with the results of Vorob'eva et al.

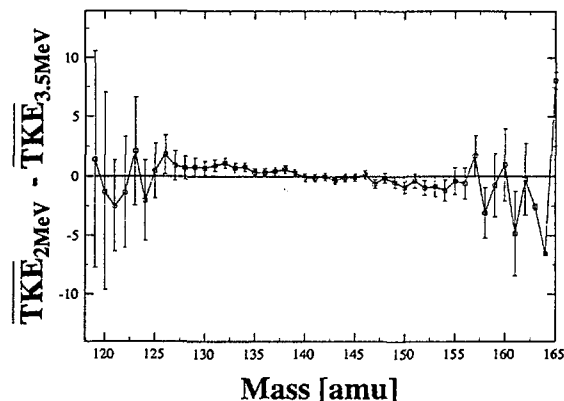


Fig. 14. Difference in TKE(A) distribution between  $E_n=2$  MeV and  $E_n=3.5$  MeV

#### The Neutron Energy Dependence of Dose Determination by BD-PND and BDT Bubble Detectors

F. Vanhavere\*, E. Wattecamps, A.J.M. Plompen

Neutron bubble detectors are becoming increasingly popular as personal dosimeters. They combine some excellent characteristics such as high sensitivity, and direct reading capability, and they are insensitive to gamma radiation.

Calibration measurements were performed at the Van de Graaff accelerator to determine the energy response of the bubble detectors. Two types of bubble detectors are used: the temperature compensated BD-PND and the BDT, both commercially available from BTI technologies in Canada. The first one has an energy threshold for neutrons at about 0.1 MeV, the second is specifically sensitive to thermal neutrons.

In a first series of experiments both types of the detectors were exposed to mono-energetic neutrons of 0.149, 0.567, 2.50 and 16.26 MeV. In a second series of calibrations some of these energies were measured again, together with new measurements with neutrons of

<sup>(1)</sup> D.L. Shpak, Sov. J. Nucl. Phys. 50 (1989) 574  
\* SCK/CEN, Mol, Belgium

0.3 and 1.2 MeV. The irradiations were done under zero degree in 1.5 m distance in free air as well as with a 30x30x15 cm<sup>3</sup> PMMA phantom on the reverse side.

Independent flux determination was done with a calibrated long counter under 45 degree at 5.335 m from the neutron target and with a calibrated Studsvik neutron detector under 45 degree at 1.99 m distance from the neutron target. In addition, for some of the highest neutron energies, fluence determination by activation measurements was also made. Neutron scattering corrections, in and out scatter, for the fluence monitors were determined with shadow bars between the target and the fluence monitors. The analysis of the data is in progress.

From the results of the investigation it will be decided whether a single BD-PND, or a combination of BD-PND and BDT bubble detectors, has a dose equivalent response. The influence of the new ICRTP 60 radiation weighting factors for neutrons will also be checked.

A paper with the following title was submitted to the International Conference on Nuclear Data for Science and Technology , Trieste, May 1997: “ Measurement of the energy dependence of dose determination with BD-PND and BDT bubble detectors in the neutron energy range from 50 keV to 16 MeV ”.

## **NUCLEAR DATA FOR FISSION TECHNOLOGY**

The objective of the work on nuclear data for fission technology is to reach a more accurate knowledge of data requested in fission research and in fission technology. Measurements cover actinide fission cross section data as well as structural material neutron interaction data. Research topics are taken to fulfil European demands collected in the NEA High Priority Request List.

### **Neutron Data of Actinides**

#### ***Investigation of the Cold Fission Fragments' Characteristics for Several Plutonium Isotopes***

L. Demattè\* , C. Wagemans\*\* , P. D'hondt\*\*\* , A. Deruytter, R. Barthélémy, J. Van Gils

In order to complete the systematic study of the fragment characteristics of the spontaneously fissioning plutonium isotopes, the cold fission (i.e. neutronless) of

---

\* EC Fellow from from University of Padova, Italy

\*\* University of Gent, Belgium

\*\*\* SCK/CEN, Mol, Belgium

$^{236,238,240,242,244}\text{Pu}(\text{SF})$  has been analysed by means of an improved method of selection of the events of interests. The neutronless fission events were identified by comparing their total kinetic energy to the Q-value of the fission reaction diminished by the neutron separation energy. This is equivalent to calculate the Q-value of the fission reaction with only one neutron emitted:

$$Q_1(A,Z) = \max \{ M(A_f, Z_f) - M(A', Z) - M(A_f - A' - 1, Z_f - Z) - M_n \}$$

where  $M(A,Z)$  is the mass excess of the isotope with mass  $A$  and charge  $Z$  (calculated from Moeller et al.<sup>(1)</sup>),  $M_n$  the mass excess of the neutron, and the maximum is chosen between all possible values of the charge splitting and  $A' = A, A-1$ . Clearly the fission events having a total kinetic energy higher than  $Q_1$  do not have enough internal energy to emit neutrons, so with this method of selection one is sure to investigate the region of neutronless fission. Further, the Q-value calculated in this way shows little or no odd-even staggering, at least compared to the Q-value of the two-body reaction, and can be used when the experimental mass resolution is higher than one. This method also gives the relative yield of the neutronless fission, i.e. the ratio between the selected neutronless events and the global number of events.

In Fig. 15, this selection criterium and a more traditional one, based on the kinetic energy of the light fragment, are compared in the case of  $^{239}\text{Pu}(n_{\text{th}},f)$ , clearly showing how much they differ in the mass symmetric and very asymmetric regions.

Keeping in mind that the present experiment is not ideal for a detailed investigation of the cold fission, the analysis is limited to only the global characteristics, summarised in Table 5. Fig. 16 shows the ratio of the relative cold fission yield  $Y_c$  and the neutronless fission probability  $P_0^{(2)}$  for  $^{236,238,240,242}\text{Pu}(\text{SF})$ . This ratio is constant within the uncertainties, allowing an estimation of the neutronless probability  $P_0 \approx 4.2\%$  for  $^{244}\text{Pu}(\text{SF})$ .

The most striking observation to be made from Table 5 is however the reduction of the cold fission yield by about one order of magnitude between  $^{240}\text{Pu}(\text{SF})$  and  $^{239}\text{Pu}(n_{\text{th}},f)$ . This points to a strong influence of the excitation energy on the cold fission yield, which is not surprising since the nuclear temperature of the fissioning system rises in the case of  $^{239}\text{Pu}(n_{\text{th}},f)$  due to the binding of the neutron.

<sup>(1)</sup> P. Moeller, J. Nix, W. Myers and W. Swiatecki, At. Data and Nucl. Data Tables 59 (1995) 185.

<sup>(2)</sup> Holden and M. Zucker, Proc; advisory Group Meeting on Nuclear Standard Reference Data, Geel 1984, Rep. IAEA-TECDOC-335 (IAEA Vienna, 1985) p.248.

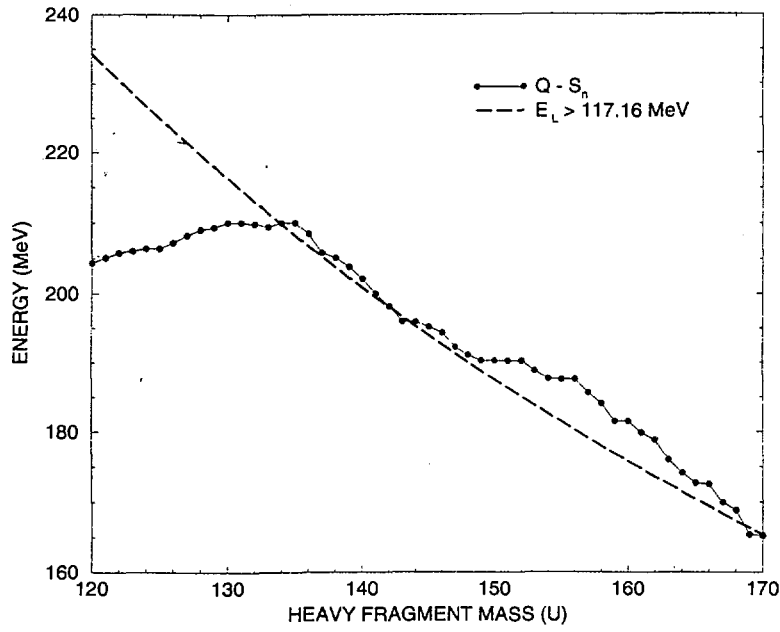
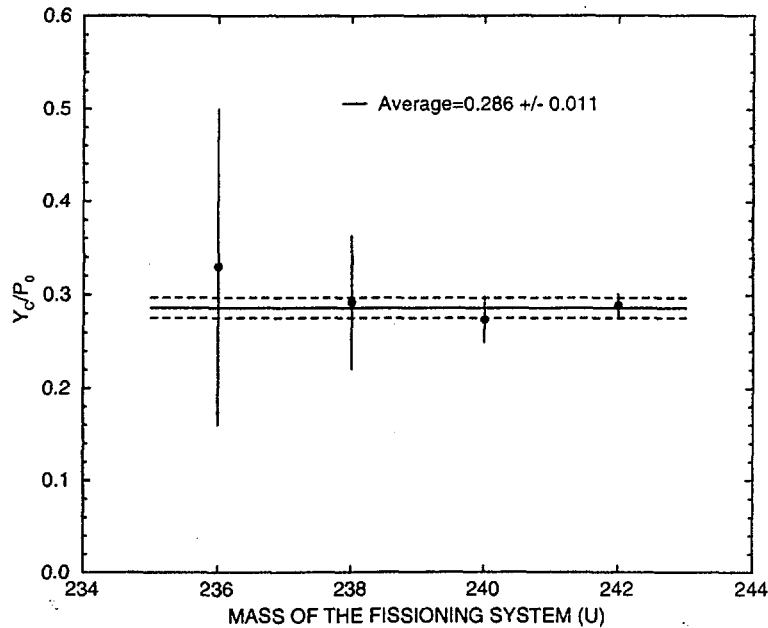


Fig. 15. Comparison between the  $Q$ -value lowered by the neutron separation energy and the total kinetic energy corresponding to a fixed value of the light fragment energy for  $^{239}\text{Pu}(n_{th},f)$

Table 5. Main characteristics of the cold fission in  $^{236,238,240,242,244}\text{Pu}(\text{SF})$  and  $^{239}\text{Pu}(n_{th},f)$

	N° of events	Rel. Yield (%)	$\langle M_h \rangle$ (amu)	$\langle E_k \rangle$ (MeV)
$^{236}\text{Pu}(\text{SF})$	49	$2.36 \pm 0.34$	$140.79 \pm 1.21$	$199.40 \pm 1.68$
$^{238}\text{Pu}(\text{SF})$	33	$1.58 \pm 0.28$	$139.53 \pm 0.88$	$197.73 \pm 1.03$
$^{240}\text{Pu}(\text{SF})$	208	$1.73 \pm 0.12$	$136.99 \pm 0.40$	$200.63 \pm 1.44$
$^{242}\text{Pu}(\text{SF})$	632	$1.961 \pm 0.079$	$136.84 \pm 0.20$	$201.54 \pm 0.24$
$^{244}\text{Pu}(\text{SF})$	213	$1.193 \pm 0.082$	$139.84 \pm 0.39$	$197.80 \pm 0.43$
$^{239}\text{Pu}(n_{th},f)$	2631	$0.1900 \pm 0.0037$	$136.41 \pm 0.14$	$205.94 \pm 0.14$



*Fig. 16. Ratio between our results  $Y_c$  and the neutronless fission probability  $P_0$*

*Influence of the Fission Modes on the Light Charged Particles Emission in Ternary Fission*

O.Serot\*, C.Wagemans\*\*, R. Barthélemy, J. Van Gils, S. Van Den Berghe, N. Carjan\*\*\*

In order to investigate the influence of the fission modes on the Light Charged Particles (LCP) characteristics, several even-even spontaneously fissioning plutonium isotopes have been studied. The set of isotopes  $^{238,240,242,244}\text{Pu}$  constitutes a very favourable case for mainly three reasons:

- the number of parameters involved during fission is reduced since fission takes place at constant (zero) excitation energy and at the same spin and parity ( $J^\pi = 0^+$ );
- the experimental conditions used to measure LCP can be exactly the same for all nuclei;
- the relative contributions of the two main fission modes i.e. Standard I and Standard II strongly vary with the nuclei (the Standard I fission mode yield increases from 6.3% for  $^{238}\text{Pu}(\text{sf})$  up to 44.5% for  $^{244}\text{Pu}(\text{sf})$ ).

A  $\Delta E$ -E detection set-up is used to measure the yield and energy characteristics of the ternary particles. A control experiment performed with  $^{252}\text{Cf}$  has shown that the well-known results of the  $^{252}\text{Cf}(\text{sf})$  were perfectly reproduced.

\* EC Fellow from University of Bordeaux, France

\*\* University of Gent, Belgium

\*\*\* Centre d'Etudes Nucléaires de Bordeaux Gradignan, France

So far binary (B) and Long Range Alpha (LRA) accompanied fission counting rates have been measured for  $^{240}\text{Pu}$ ,  $^{242}\text{Pu}$  and  $^{244}\text{Pu}$ . Energy spectra for these three isotopes are shown in Fig. 17. The  $^{238}\text{Pu}(\text{sf})$  data taking is still going on. Up to now, a significant increase of the LRA emission probability per binary fission (LRA/B) has been found with increasing Standard II mode yield suggesting that the LRA emission probability is influenced by the deformation of the system at scission since the Standard II mode corresponds to a more elongated system than the Standard I mode (Fig. 18). This result confirms the general idea that the energy required to release LCP is taken from the deformation energy of the scissioning system.

LRA characteristics are also under investigation for a series of  $^{239}\text{Pu}(\text{n},\text{f})$  resonances. The experimental work is carried out at an 8.5 m flight path of GELINA. A double symmetric  $\Delta E$ -E detection set-up is used as described by S. Pommé et al.<sup>(1)</sup>. The geometrical configuration of the ionisation chamber is the same as for spontaneous fission measurements. Possible variations of LRA/B ratios amongst the resonances might reveal correlations with the respective fission mode contributions and with other resonance characteristics.

The impact of the deformation of the fissioning nuclei on the LRA emission probability is studied theoretically using the mechanism of the non-adiabatic ejection of the LRA<sup>(2)</sup>. This approach is related to a fast change in the nuclear potential during the scission stage. The emission probability and the energy of the LRA can be deduced by expanding the wave function defining LRA before scission in the set of eigen functions of the system immediately after scission. This can be justified for LRA since the potential changes during the neck rupture much are than the period of motion of the  $\alpha$  particle cluster. The comparison between the theoretical results obtained in this way with our corresponding experimental data will be done in a nearby future.

---

<sup>(1)</sup> S. Pommé et al. Nucl. Instr. And Meth. A 359 (1995) 587

<sup>(2)</sup> I. Halpern, Annu. Rev. Nucl. Sci., 1971, vol. 21

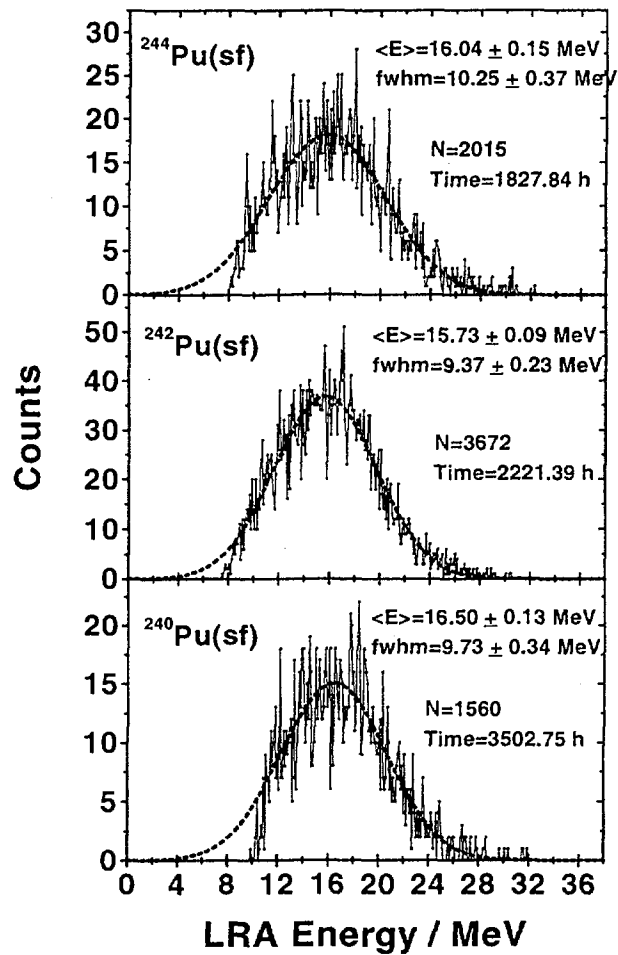


Fig. 17. LRA spectra for  $^{240,242,244}\text{Pu}(sf)$ . The total number of counts and measuring time is indicated on each plot. All the Gaussian fits were done from 12.5 MeV on

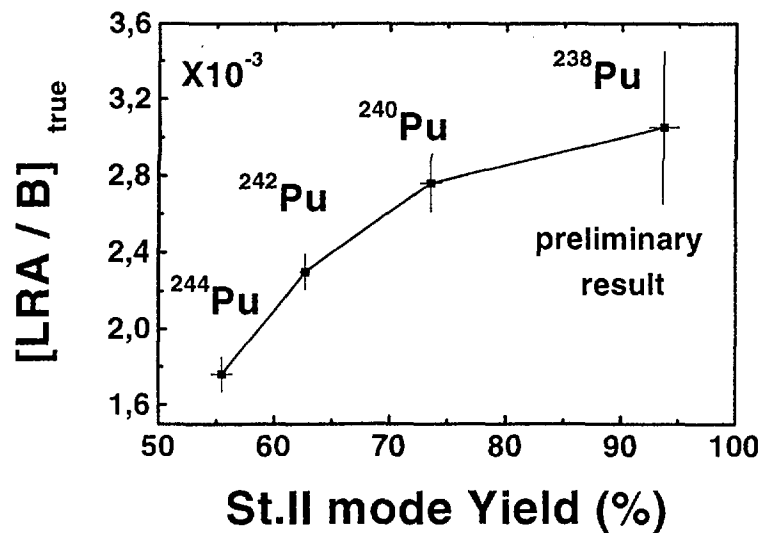


Fig. 18. Correlation between LRA/B and the Standard II fission mode yield

## Neutron Data of Structural Materials

### *High Resolution Inelastic Scattering Cross Section of $^{23}\text{Na}$ and $^{27}\text{Al}$*

S. Kopecky, R. Shelley, H. Märten\*, H. Weigmann

The inelastic cross sections of selected light elements have been measured in high resolution time of flight experiments at the Geel pulsed electron linear accelerator (GELINA). The accelerator was run at optimum conditions of 1 ns pulse width 800 Hz repetition rate and a mean electron beam current of 50  $\mu\text{A}$  for several weeks. The source of white neutrons emerging from a rotary uranium target was used for the measurements at a neutron flight path of 58.5 m and the neutron flux was constantly monitored at 27.5 m with a  $^{235}\text{U}$  fission chamber. Neutrons and  $\gamma$ -rays emitted in inelastic neutron scattering were detected by a system of eight NE213 liquid scintillators and sorted by pulse shape discrimination. Detector responses were calculated by Monte Carlo techniques.

For  $^{23}\text{Na}$  the inelastic scattering was measured for the first level at 440 keV. Data up to 2 MeV were analysed with the R-matrix code SAMMY to extract resonance parameters. Simultaneously the total cross section data of Oak Ridge were fitted with the same set of parameters.

For  $^{27}\text{Al}$  the inelastic scattering from the first two levels, at 843 keV and 1015 keV, could be separated. The cross section for these two levels show different resonance structures, due to the angular momentum coupling. The analysis above the inelastic threshold up to approximately 2 MeV, again using SAMMY, combined this inelastic data with total cross section data measured at GELINA.

### *High Resolution Measurement of the Neutron Inelastic Scattering Cross Section of $^{56}\text{Fe}$*

E. Dupont, P. Ribon, H. Weigmann, G. Vanpraet\*\*

High resolution inelastic scattering cross section measurements have been carried out on an enriched  $^{56}\text{Fe}$  sample in the energy region from threshold up to about 3 MeV.

The experiments were performed using the time of flight technique on the 200 m flight path at the GELINA with a neutron burst widths of less than 2 ns. Four  $\text{BaF}_2$  scintillators set around the sample at  $90^\circ$  scattering angle detected the emitted  $\gamma$ -rays.

---

\* Visiting Scientist from the TU Dresden, Germany

\*\* RUCA, Antwerp, Belgium

The  $^{10}\text{B}(n,\alpha\gamma)$  reaction from a boron disk covering the front side of the iron one was used to monitor the neutron flux and to normalise the cross section.

The data are being analysed together with iron transmission by means of the R-matrix code SAMMY. The aim of this analysis is to determine the correlation between neutron elastic and inelastic partial widths.

***Total Neutron Cross Section Measurements of  $^{10}\text{B}$  at Some Energy Points Between 0.4 and 1.9 MeV***

A. Crametz, A.J.M. Plompen, W. Schubert, E. Wattecamps

Measurements of the total neutron cross section of  $^{10}\text{B}$  were performed in 1994 at the GELINA- and at the Van de Graaff- accelerators from 80 eV to 100 KeV and from 1.5 to 18 MeV, respectively. The data were reported at the International Conference on Nuclear Data for Science and Technology in Gatlinburg, Tennessee, May, 1994. (p. 47). Comparison of these data with similar measurements performed at ORNL have shown that the three sets of measurements are coherent, but different from the ENDF/B-VI standards cross section file. The measured values are 5 % larger at .2 MeV and 4 % smaller at 1.0 MeV. The measurements at ORNL and IRMM are made with different  $^{10}\text{B}$  samples and provide independent absolute values. The measurements of ORNL were made in a single run from .1 to 20 MeV, but the measurements at IRMM were made in two separate energy ranges with an energy gap from .1 to 1.5 MeV. In this range the discrepancy between the measurements and the ENDF/B-VI values is largest. Therefore new measurements were performed at IRMM.

The background determinations in the older measurements were done by the black resonance or black plug transmission technique, but now it was preferred to apply the time-of-flight technique with mono-energetic neutrons from a thin target at the pulsed Van de Graaff accelerator. The background underneath the time of flight peak of the mono-energetic source is determined by interpolation of the background level just previous and just after the mono-energetic peak. This technique is independent from earlier background determination techniques, but time consuming, and therefore limited to a small number of single energy points between .4 and 1.9 MeV. (9 energies performed already and two more are planned).

Key words for the experimental set up described earlier are essentially as follows: T(p,n) target reaction,  $0.4 \text{ mg/cm}^2$  TTi, neutron burst width 2 ns, flight path 4m, four copper collimators of 30 cm length each, well shielded NE213 of 10 cm diameter and 2.5 cm

thickness, sample changer with three sample positions (no sample,  $^{12}\text{C}$  and  $^{10}\text{B}$ ). Particular care was devoted to check the normalisation of the neutron yield of the accelerator. Three independent fluence monitors are compared at 600 s intervals to within the level of statistical accuracy of  $< 0.3\%$ . The pulse shape discrimination circuit of the NE213 detector was checked frequently. Critical analysis of raw data and subsequent analysis's were made easy and fast with new acquisition programmes. As in 1994 total cross section measurements of  $^{12}\text{C}$  were performed in parallel, thus testing the reliability of the measurement and analyses.

Results from the recent measurements of  $^{12}\text{C}$  and  $^{10}\text{B}$  are shown in Fig. 19 as cross section ratios of measured- to evaluated ENDF/B-VI- values. The measurements of ORNL for  $^{10}\text{B}$ , are also shown in Fig. 19. Measurements at single energies were repeated at least nine times in 600 s intervals and each interval is considered as a separate measurement. The mean deviation of these cross section data from the mean is scattering between 0.9% at best and 1.3 % in the worst case. The measured  $^{12}\text{C}$  data are lower than the ENDF/B-V values, mean deviation approximately 1.3%. Recent  $^{10}\text{B}$  data confirm the previous deviation from the ENDF/B-VI set and the trend of the deviation measured by ORNL as well. Further analysis is in progress to care in more detail for small multiple scattering corrections and dead time losses. Numerical values with best estimates for error bars will be submitted at the International Conference on Nuclear Data for Science and Technology in May 1997 in the communication with the following title: "Total neutron cross section measurements of  $^{10}\text{B}$ ".

### *Study of the $^{17}\text{O}(n,\alpha)^{14}\text{C}$ Reaction with Thermal Neutrons*

C. Wagemans\*, J. Wagemans\*, R. Bieber\*\*, P. Geltenbort\*\*\*, R. Barthélémy

The formation of elements heavier than  $A=17$  in inhomogeneous big-bang scenario's critically depends on the  $^{17}\text{O}(n,\alpha)^{14}\text{C}$  reaction , its cross-section value for thermal neutrons being decisive.

---

\* University of Gent, Belgium

\*\* EC fellow from the Technical University of Vienna, Austria

\*\*\* Institut Laue-Langevin, Grenoble, France

In order to determine this cross-section accurately, a measuring technique using gaseous oxygen samples (with a 65.2% enrichment in  $^{17}\text{O}$ ) and a surface barrier detector has been developed. The neutron flux is determined correspondingly relative to the  $^{14}\text{N}(n_{\text{th}},p)$  cross-section, for which a value of  $(1.83 \pm 0.03)\text{b}$  was adopted. The method has been optimised during test measurements at the high flux reactor of the Institut Laue-Langevin in Grenoble.

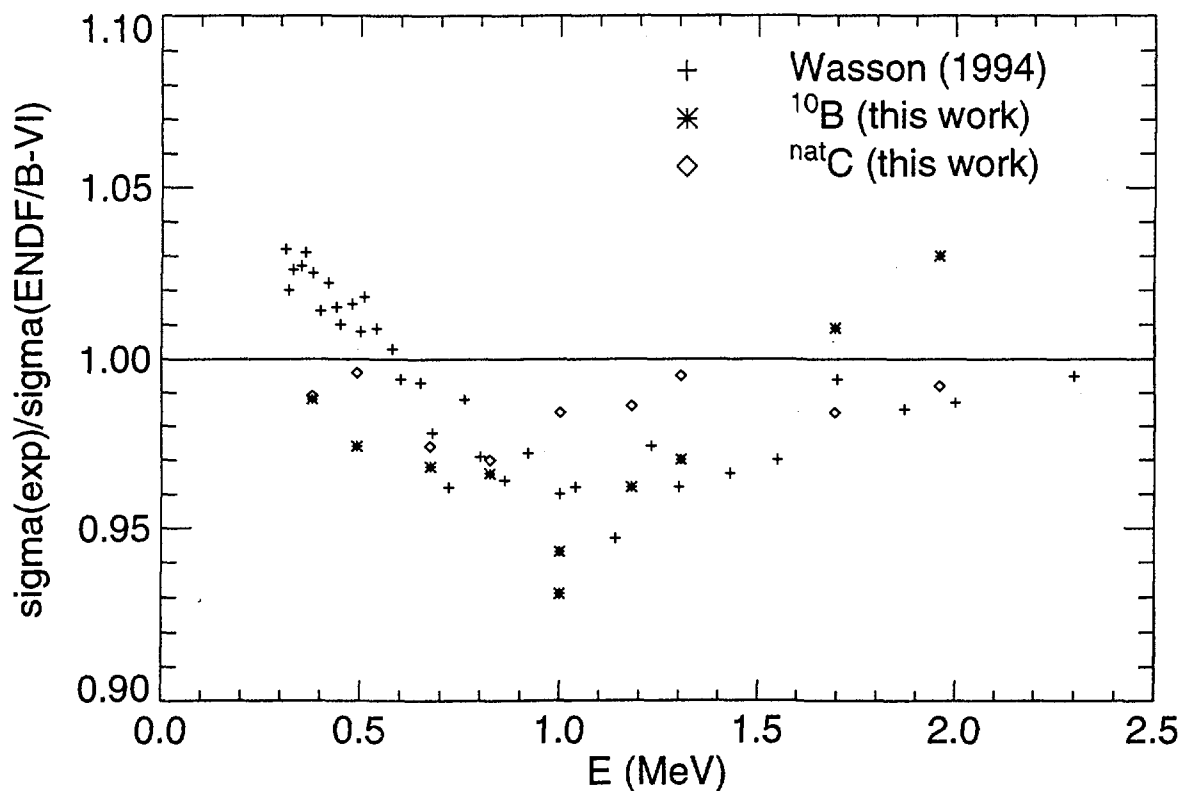


Fig. 19. Ratio of measured data to evaluated values of total cross section for  $^{10}\text{B}$  and  $^{12}\text{C}$  as a function of neutron energy

## SPECIAL STUDIES

Some special measurements linked to the data programme has been performed. These research topics concerned PhD work as well as extended international collaboration making use of the unique features of GELINA as a high energy-resolution machine for neutron measurements.

### *Determination of (n,p) and (n,α) Cross-Sections Influencing the Nucleosynthesis of $^{36}\text{S}$*

R. Bieber\* , C. Wagemans\*\* , R. Barthélémy, J. Van Gils

$^{36}\text{Cl}(n,p)^{36}\text{S}$  is one of the key-reactions leading to the production of the rare isotope  $^{36}\text{S}$  in stellar nucleosynthesis. The lack of reliable experimental cross-section data however introduces important discrepancies in the corresponding nucleosynthesis network calculations.

Last year the  $^{36}\text{Cl}(n,p)^{36}\text{S}$  and the competing  $^{36}\text{Cl}(n,\alpha)^{33}\text{P}$  reactions were studied. The measurements were performed at two flight paths of the linear accelerator GELINA. The data taking at the 9 m flight path was finalised, but at 30 m the measurements are being continued. The detector was a grided gas flow ionisation chamber using very pure  $\text{CH}_4$ -gas. Under these conditions the reaction cross-sections have been measured with high resolution from 1 eV up to 300 keV. The neutron flux was determined by means of the  $^{10}\text{B}(n,\alpha)^7\text{Li}$  reaction. The background was measured with black resonance neutron filters. By choosing suited sample thickness and detection conditions the (n,p) and (n,α) reactions could be separated nicely. Only the resonance at 932 eV shows a dominant α-contribution of about 60 %. For most resonances this contribution is only a few %, rising to some 20 % for the 82.5 keV resonance.

With the measured cross-sections preliminary values for the corresponding astrophysical reaction rate and the Maxwellian averaged cross-section were calculated.

Another interesting isotope in this scenario is  $^{37}\text{Ar}$ . Determining the  $^{37}\text{Ar}(n,p)^{37}\text{Cl}$  and  $^{37}\text{Ar}(n,\alpha)^{34}\text{S}$  cross-sections was quite a challenge in view of the short half-life of only 35.04 d and of the problems related to the sample preparation. The  $^{37}\text{Ar}$ -samples were produced at the Cyclotron in Louvain-la-Neuve. However, the efforts appear to be

---

\* EC fellow from the Technical University of Vienna, Austria

\*\* University of Gent, Belgium

worthwhile, since preliminary results reveal the existence of a few extremely strong resonances in the keV-region, with peak cross-sections of several hundred barns!

In the beginning of 1997 a thicker  $^{37}\text{Ar}$ -sample is planned to be produced in order to determine the thermal cross-sections at the ILL in Grenoble and the resonances at the GELINA.

### *The Stellar Capture Rate of $^{136}\text{Ba}$*

P. Mutti\*, F. Corvi, K. Athanassopoulos, H. Beer\*\*

The barium isotopes and more particularly the nuclides  $^{134,136}\text{Ba}$  represent a notable exception in the field of the *s*-process nucleosynthesis. In fact, *s*-process calculations yield a barium overproduction of at least 20% of the known solar abundance. There are two possibilities to explain these discrepancies: either the stellar capture rates of  $^{134,136}\text{Ba}$  and/or the solar barium abundance are systematically more uncertain than previous believed; or the current *s*-process models have deficiencies which become evident in the region around the exposure-sensitive bottleneck isotope  $^{138}\text{Ba}$ . In an effort to thoroughly investigate the first point, the  $^{136}\text{Ba}$  capture cross section was measured with high resolution at the Geel electron linac. The sample, consisting of 13.76 gr. of  $\text{BaCO}_3$  enriched to 92.677% of  $^{136}\text{Ba}$ , was placed at a 28.41 m flight distance and capture  $\gamma$ -rays were detected by two cylindrical  $\text{C}_6\text{D}_6$ -based liquid scintillators placed perpendicularly to the neutron direction at 4 cm from the sample centre. The measurement time of the main run was 330 hours. The data were normalised to silver capture at 5.19 eV using the saturated resonance method. The data were analysed with the R-matrix shape-fitting code REFIT taking as a fixed input the neutron width values determined in a recent transmission measurement<sup>(1)</sup>. In this way values of the capture areas were derived for 184 resonances in the energy range up to 60 keV. Considering only the resonances for which a firm *l*-assignment was given<sup>(1)</sup> the average and the standard deviation  $\sigma$  of the distribution of *s*- and *p*-wave radiative widths  $\Gamma_\gamma$  were calculated respectively. These values are compared in Table 6: the present average values for *l*=0 and *l*=1 resonances are respectively ~ 28% and ~ 12% lower than the ORLN data. The Maxwellian-Averaged capture Cross section (MAC) values calculated from the present data, and supplemented<sup>(1)</sup>

---

\* EC Fellow from the University of Torino, Italy

\*\* Forschungszentrum, Karlsruhe, Germany

<sup>(1)</sup> P. Koehler et al., Phys. Rev. C54, 1463 (1996)

for the region above 60 keV, are listed in Table 7 together with the corresponding values recently obtained in Karlsruhe<sup>(1)</sup> and Oak Ridge<sup>(2)</sup>. To conclude, the present results rule out the possibility of explaining the barium excess with a change in the capture rate. Since also 20% variation of the meteoritic abundances is highly unlikely, the solution may be found in *s*-process scenarios more sophisticated than those used up to now.

**Table 6. Comparison of  $\langle \Gamma_\gamma \rangle$  values for *s*- and *p*-waves**

<i>l</i>	Present Work		Koehler <i>et al.</i> <sup>(1)</sup>	
	$\langle \Gamma_\gamma \rangle$ (meV)	$\sigma$ (meV)	$\langle \Gamma_\gamma \rangle$ (meV)	$\sigma$ (meV)
0	62.6	14.8	86.9	29.2
1	172.0	65.5	196.2	52.7

**Table 7. Maxwellian-Averaged neutron capture cross section**

KT (keV)	$\langle \sigma V \rangle / VT$ (mb)		
	Present Work	Voss <i>et al.</i> (2)	Koehler <i>et al.</i> (1)
5	166.3 ± 4.9		186.0 ± 6.1
8	124.2 ± 4.5		139.4 ± 4.5
10	108.6 ± 4.0	109.7 ± 4.6	122.0 ± 3.9
12	97.7 ± 3.8	99.3 ± 3.9	
15	86.2 ± 3.6		94.6 ± 3.0
20	74.1 ± 3.3	74.9 ± 2.7	79.2 ± 2.5
25	66.2 ± 3.1	66.5 ± 2.3	69.2 ± 2.2
30	60.4 ± 2.9	60.6 ± 2.1	62.0 ± 2.0

**Measurement of the Neutron Total and Capture Cross Section of <sup>99</sup>Tc in the Energy Range from 0.1 to 100 keV**

C. Bastian, A. Brusegan, F. Corvi, G. Fioni\*, F. Gunsing\*, A. Leprêtre\*, E. Macavero, C. Raepsaet\*

In order to improve nuclear data for waste transmutation purposes, a project within the framework of a collaboration between the Institute for Reference Materials and Measurements (IRMM) and the French Commissariat à l'Energie Atomique (CEA) has been started to measure neutron cross sections. The first isotope under study is <sup>99</sup>Tc.

<sup>(1)</sup> P. Koehler *et al.*, Phys. Rev. C54, 1463 (1996)

<sup>(2)</sup> F. Foss *et al.*, Phys. Rev. C52, 1102 (1995)

\* CEA Saclay, Gif sur Yvette, France

In 1995 the total and capture cross sections of  $^{99}\text{Tc}$  have been measured in the 3 to 600 eV energy range. These data are currently being analysed. In 1996 both total and capture cross sections of  $^{99}\text{Tc}$  have been measured in the 0.1 to 100 keV neutron energy range. For the capture experiment a  $1\text{ g/cm}^2$  thick sample and two  $\text{C}_6\text{D}_6$  total energy gamma-ray detectors with a pulse height weighting method were used. Data were taken with a transputer based data acquisition system. The transmission experiment was done with a  $4\text{ g/cm}^2$  thick sample the FAST data acquisition system. The raw data of both experiments are reduced into cross sections with the AGS package and a resonance parameter analysis is being performed using the shape codes REFIT and SAMMY.

***Measurement of the (n,n' $\gamma$ ) Excitation Functions of Low Lying Levels of Molybdenum Isotopes***

I.-G. Birn\* , E. Wattecamps, H. Weigmann

The fast neutron spectrum and the reactivity in a fission reactor are sensitive to inaccuracies of inelastic scattering cross section data. New measurements of inelastic scattering cross sections for fissile, fertile, structural materials and for fission products as well are required<sup>(1)</sup>.

Measurements of  $\gamma$ -ray production cross sections were performed at the Van de Graaff laboratory for palladium earlier<sup>(2)</sup> and more recently for molybdenum inelastic neutron cross sections for some levels were deduced. A pulsed white neutron source was used and two-dimensional spectra of  $\gamma$ -ray energy versus incident neutron energy were recorded. A detailed description of the experiment including data analysis and discussion of results is in preparation. Numerical values for cross sections of some single levels (first, second or third) of  $^{92}\text{Mo}$ ,  $^{98}\text{Mo}$  and  $^{100}\text{Mo}$  were submitted for evaluation. A pulsed proton beam of 1.5 ns burst width and 5.5 MeV energy impinges on a thick (1 mm) natural lithium target, thus providing a broad and smooth spectrum up to the maximum neutron energy of 3.5 MeV. A  $^{\text{nat}}\text{Mo}$  disk of 7.0 cm diameter and 3mm thickness is set at 4.08 m distance from the target in the forward direction. On the reverse side of the molybdenum sample there is a sintered  $\text{B}_4\text{C}$  sample of 7.0 cm diameter and  $0.399\text{ g }^{10}\text{B/cm}^2$ .

---

\* SAP, Waldorf, Germany

(1) WRENDA 93/94 World Request List for Nuclear Data, INDC(SEC)-104

(2) A.Meister, G. Rollin, W. Schubert and E. Wattecamps, in Proc. Int. Conf. on Nuclear Data for Science and Technology, Gatlinburg (1994), p. 263

The sample plane is turned at 45 degree relative to the neutron beam. A HPGe (75 cm<sup>3</sup>, 5 cm diameter, 4 cm height) is set under 90 degree well outside the direct beam and surrounded by a heavy shield. The time resolution of the HPGe detector is 6 ns and the energy resolution is about 2.5 keV. Data were stored in list mode using the programme LISA and were analysed off-line. Data acquisition is done in 20 runs of approximately 4 hours each. After data reduction is performed and some additional checks for neutron background are made, the  $\gamma$ -ray production cross section  $\sigma_\gamma$  in each energy bin is calculated by the following formula:

$$\sigma_\lambda = \frac{C_{Mo} - (1 \div \alpha)}{C_B - f_{higherEn}} \cdot \frac{N_B}{N_{Mo}} \cdot \frac{\epsilon_B}{\epsilon_{Mo}} - f_{aniso} - f_{scatter} - \sigma_{ref}$$

$C_{Mo}$	counts of the Mo $\gamma$ -line from inelastic neutron scattering, all background contributions subtracted
$\alpha$	the conversions coefficient of the Mo $\gamma$ -line
$C_B$	counts from the $^{10}\text{B}(n,\alpha\gamma)$ reaction, all background contributions subtracted
$N_{Mo}$	number of nuclei of the considered Mo isotope per irradiated sample area
$N_B$	number of $^{10}\text{B}$ nuclei per irradiated sample area
$f_{higherEn}$	correction to the $^{10}\text{B}(n,\alpha\gamma)$ count rate due to neutrons scattered from higher neutron energy bins into the bin considered
$\epsilon_B$	HPGe detector efficiency for the 478 keV $\gamma$ -line from $^{10}\text{B}(n,\alpha\gamma)$
$\epsilon_{Mo}$	HPGe detector efficiency of the $\gamma$ -line from Mo( $n,n'\gamma$ )
$f_{aniso}$	correction for the conversion of 90 degrees yield data to $4\pi$ sr yield
$f_{scatter}$	correction for multiple scattering and absorption in the Mo and B samples
$\sigma_{ref}$	the reference cross section of the $^{10}\text{B}(n,\alpha)$ reaction

The  $\gamma$ -ray detection efficiency versus  $\gamma$ -ray energy was determined by experiment with a standardised multi- $\gamma$ -ray reference source with the same area as the molybdenum sample. The self absorption of the  $\gamma$ -rays in molybdenum was determined by 7 calibrations, sliding the reference  $\gamma$ -source inside the molybdenum layers made of 6 disks of 0.5 mm each. Similarly, but less differential in thickness, the measurements for the  $^{10}\text{B}$  line were made with the reference source in front and in the back of the  $^{10}\text{B}$  sample. The multiple scattering correction  $f_{scatter}$  (but still in proper time bin) was calculated by MCNP calculations. The correction factors are in the order of 5 to 10 % and their uncertainty taken as 30 %.

The scattering correction factor  $f_{higherEn}$  which is due to higher neutron energies detected late, but heavily weighed by the  $1/v$  cross section of  $^{10}\text{B}(n,\alpha\gamma)$  was calculated and amounts to 5 % or less for the  $^{10}\text{B}$  reaction rate.

The anisotropy corrections needed to extend the measured 90 degree cross section to cross sections integrated over  $4\pi$ sr were calculated. The calculation is based on a calculated angle dependent efficiency (MCNP). The angular distribution of the  $\gamma$ -rays from inelastic

scattering were calculated according to the model of E.Sheldon and D.M.Patter<sup>(1)</sup>. Corrections are 10 to 15 %, with an estimated uncertainty of 30 %.

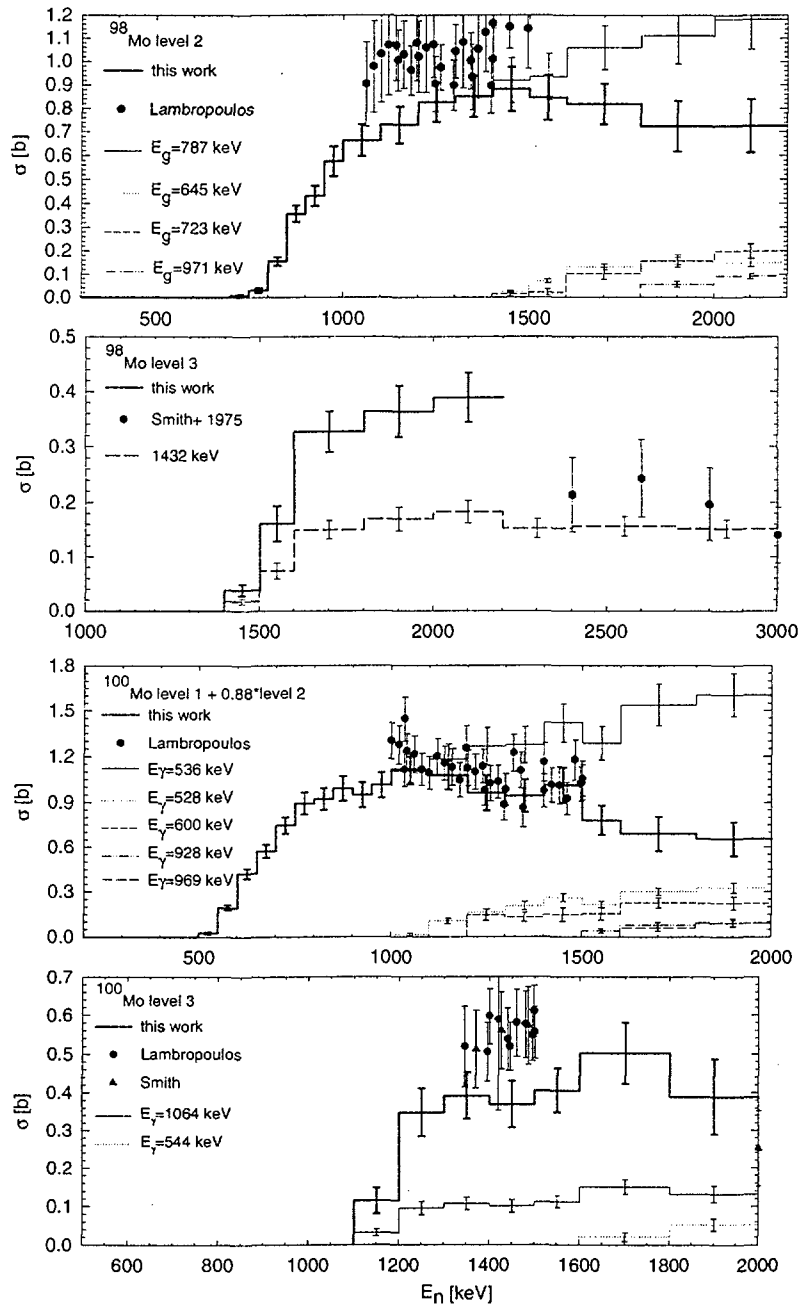


**Fig. 20. Excitation functions for some levels in different molybdenum nuclides:**

- a)  $^{98}\text{Mo}$ , 1509 keV,  $E_n$  up to 3.0 MeV
- b)  $^{98}\text{Mo}$ , 787 keV,  $E_n$  up to 2.0 MeV
- c)  $^{98}\text{Mo}$ , 1432 keV,  $E_n$  up to 2.2 MeV
- d)  $^{100}\text{Mo}$ , 536 and 695 keV,  $E_n$  up to 2.2 MeV
- e)  $^{100}\text{Mo}$ , 1064 keV,  $E_n$  up to 1.8 MeV

<sup>(1)</sup> E. Sheldon and D.M.V. Patter, "Compound inelastic nucleon and gamma-ray angular distribution for even- and odd-mass nuclei", Rev. Mod. Phys. 38 (1966) 143

The cross section for inelastic scattering of specific nuclear levels is deduced from the  $\gamma$ -ray production cross sections by subtracting all contributions due to higher levels feeding the specific level. The excitation functions for the some levels are shown in Fig. 20, together with some  $\gamma$ -ray production cross sections, and where possible are compared with data from literature. The data confirm previous results or indicate smaller values by about 20 %. A paper with more details is submitted for presentation at the International Conference on Nuclear Data for Science and Technology, Trieste, May 1997.

***The Investigation of Doppler Broadening of Neutron Resonances at Different Temperatures***

P. Siegler, P. Ribon\*, A. Meister\*\*, H. Weigmann, C. Bürkholz, C. Van der Vorst, Z. Hudson

An experimental set-up for the investigation of the temperature dependent shape of neutron resonances is installed at the pulsed white neutron source GELINA. High resolution neutron time-of-flight measurements are made using a flight path length of 26.5 m, giving a resolution better than 15 meV at 6 eV. The neutrons are measured by a  $^6\text{Li}$ -glass scintillator mounted between two photomultiplier tubes. Modifications of the signal path and the signal processing improved the deadtime as well as the stability of the pulses. Special effort has been made to investigate the origin and the amount of neutron background.

The samples are mounted in a cryostat, allowing stabilised temperatures in the range of 13 Kelvin up to 300 Kelvin. For the measurement of transmission spectra and comparing measurements between different samples, the cryostat is mounted on a sample changer.

A first set of measurements for the low lying  $^{238}\text{U}$  resonances was finished using U and  $\text{UO}_2$  samples. The interpretation by an lattice vibration model showed superior results compared to an effective gas model

The experiments with monocrystalline  $\text{Hg}_2\text{Cl}_2$  samples are concluded for different crystal orientations and temperatures from 24 Kelvin to 300 Kelvin. Special emphasis has been given to the phase transition at 185 Kelvin. The raw data is processed and the final analysis is ongoing. The experimental investigation for tantalum and  $\text{UO}_3$  has already started.

---

\* Visiting Scientist from CEA-Saclay, France

\*\* Visiting Scientist from the Technical University of Dresden, Germany

The high temperature furnace, constructed at ILL Grenoble, is completed and tests at 2000 Kelvin have been done. The preparation for the installation at IRMM has started. The  $\text{UO}_2$  monocrystals, being used for the experiment up to 3000 Kelvin are orientated and sliced.

*Measurement of the  $^{238}\text{U}(n,n')$  Cross Section between 2.0 and 3.5 MeV*

C. Goddio\*, A. J. M. Plompen, E. Wattecamps

Measurements of the  $^{238}\text{U}(n,n')$  cross section for incoming neutron energies from 2.0 to 3.5 MeV and excitation energies between 0.5 and 1.5 MeV are ongoing at the Van de Graaff laboratory. During the present reporting period a series of runs were performed at the accelerator varying a number of parameters and dispositions. This was done to find out by experiment and by Monte Carlo calculations the optimum measuring conditions that can be achieved with the equipment presently available.

On the basis of investigations performed under  $90^\circ$  the set-up was extended to spectrometers at  $35^\circ$ ,  $55^\circ$  and  $125^\circ$  to get a better measure of the total inelastic cross section. The first run with this set-up was performed in December 1996.

Neutrons are produced by the  $\text{T}(p,n)^3\text{He}$  reaction at the 7 MV Van de Graaff accelerator using a  $\text{Ti}(T)$  target of  $0.47 \text{ mg/cm}^2$  thickness. The  $^{nat}\text{U}$  sample is a hollow cylinder of 3.5 cm outer diameter, 1.6 cm inner diameter and 2.5 cm height placed in 12 cm distance from the target. Similar  $^{nat}\text{C}$  and polyethylene samples are used for normalisation. The flight path length from scatterer to detector is 1.8 m. Neutron Time Of Flight- (TOF), pulse height- and pulse shape- spectra of the three NE213 detectors are recorded simultaneously. The detector dimensions are 10 cm diameter and 2.5 cm thickness. The monitors are an additional NE213 liquid scintillator operating in TOF mode with Pulse Shape Discrimination (PSD), a Pilot-U plastic scintillator also in TOF mode, a lithium glass detector and a current integrator. The efficiency of the main detectors will be determined relying on the known angular differential neutron production cross sections for the  $\text{T}(p,n)^3\text{He}$  reaction. This type of procedure was already adopted for one detector in the energy range from 0.6 MeV to 2 MeV and compared with Monte Carlo calculations. Fig. 21 shows TOF spectra of the  $55^\circ$  detector observed with and without the  $^{nat}\text{U}$  sample in place at an incident neutron energy of 1.8 MeV. Both spectra are obtained after PSD and normalisation to the same fluence, but not yet corrected for the detector efficiency.

---

\* EC Fellow from the University of Torino, Italy

The acquisition time is about 100 minutes. The peak observed without sample is due to both the sample support structure and the direct beam. An additional reduction of the direct beam component was achieved after this measurement. Longer runs are needed to get sufficient statistical accuracy. In January 1997 measurements at neutron energies of 2.0, 2.5, 3.0 and 3.5 MeV are planned. The results of these measurements corrected for fission neutrons, multiple scattering and  $^{235}\text{U}$  contributions will be compared with current evaluated data files and theoretical calculations. A paper will be presented at the Nuclear Data for Science and Technology Conference in Trieste (May 97).

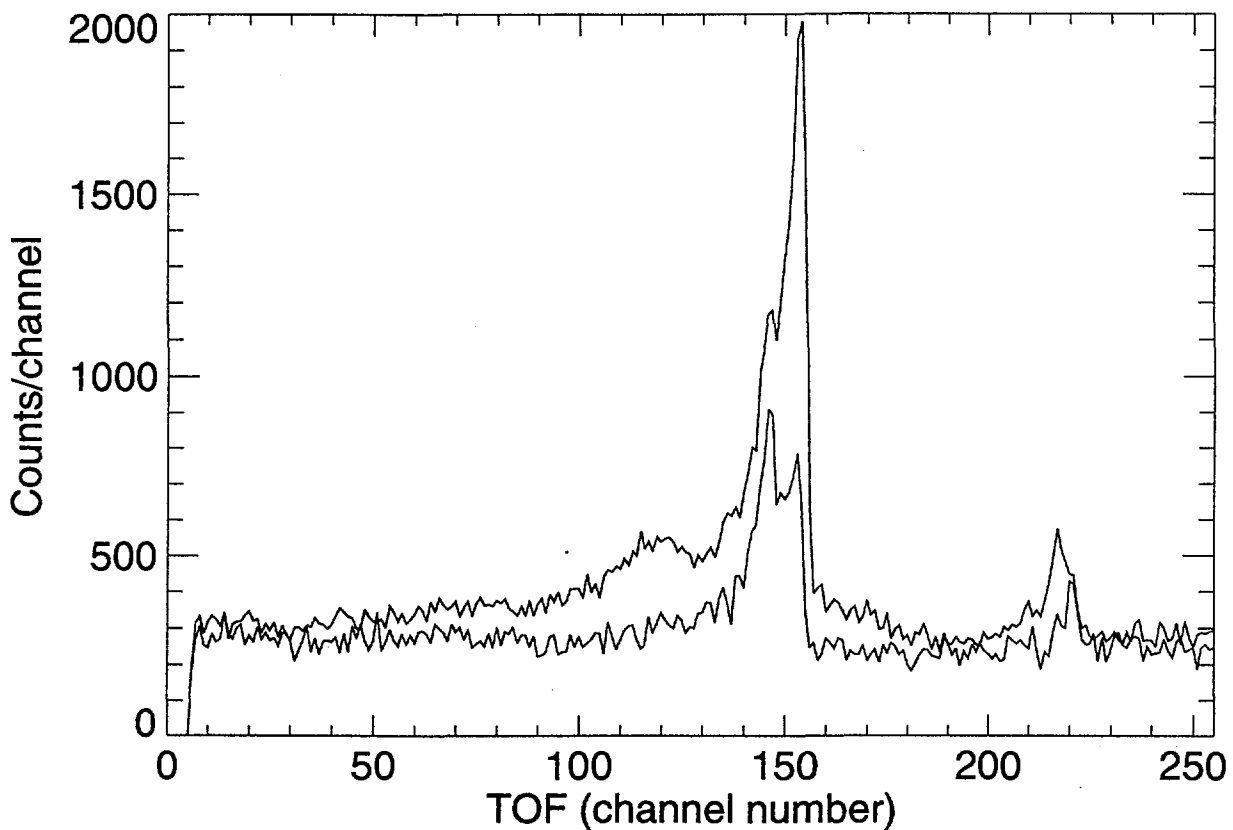


*Fig. 21. Typical TOF spectra taken at 55° spectrometer position (1.44 ns/channel)*

***$^{208}\text{Pb}$  Inelastic Neutron Scattering Cross Section Measurement***

S. Kopecky, R. Shelley, C. Bastian, C. Nazareth

Neutron emission cross sections of lead are requested for fusion reactor blanket calculations and for the study of possible lead cooled fast reactors. GELINA is run at 800Hz with 1ns neutron pulses and neutron energies are determined by the TOF technique at 60m flight length. At this distance the enriched  $^{208}\text{Pb}$  sample is surrounded by eight NE213 liquid scintillators and photomultipliers and pulse shape discrimination is used to distinguish between scattered neutrons and gamma rays. Each detector pulse, both the

neutron and the gamma pulses and signals coming from a  $^{235}\text{U}$  fission chamber sited in the beam at 30m, are tagged ( 11 in total) and fed to the acquisition system.

Until recently measurements of neutron emission cross sections by time of flight (TOF) have been performed using ND6600 data acquisition systems. After a first in-house multi-parameter transputer based acquisition system<sup>(1)</sup> had been used, a similar, but extended, system has been built and installed to replace the ND6600's for these measurements.

The heart of the system consists of a 0.5ns time coder/multiplexer through which up to 11 TOF signals can be routed and coded by a 16-bit transputer and then analysed by two 32-bit transputers directly linked to a microVAX computer. Here, resulting histogram and list data files are built up and temporarily stored together with relevant amplitude spectra. Canberra's Genie Enhanced Spectroscopy Package has been installed for graphical display and measurement specific control software routines have been written.

Extensive data collection is expected to start early in 1997 as soon as all parts of the experiment have been fully tested.

### *Spin and Parity Assignment of $^{109}\text{Ag}$ Neutron Resonances*

L. Zanini\*, F. Corvi, K. Athanassopoulos, H. Postma\*\*

In the frame of the TRIPLE collaboration for the study of parity violation in neutron resonances, an experiment of spin assignment of  $^{109}\text{Ag}$  neutron resonances was carried out. The knowledge of the spins allows a better determination of the root-mean squared parity-violating matrix element M, from which the strength of the weak interaction in the compound nucleus can be derived.

The experimental installation at a 12.8 m flight distance, consisted of two coaxial Ge-detectors, placed symmetrically with their axis at an angle of 30 degrees with respect to the sample plane. The sample was a silver metal disc of 10 cm diameter enriched to 97.1 %  $^{109}\text{Ag}$ . Capture gamma-rays were measured in the range 0.1-6.9 MeV with two 8k ADC in the neutron energy range from 10 to 1400 eV, collecting a total amount of 40 Gbytes of listing data over a period of 1200 hours. The low-level population method of spin assignment was applied using in some cases additional information from primary gamma-rays.

---

<sup>(1)</sup> IRMM Annual Report 94, EUR 16273 EN

\* EC Fellow from University of Torino, Italy

\*\* University of Delft, The Netherlands

For s-wave resonances the ratio between the gamma-rays at 338.9 and 350.1 keV was taken, which are not very strong but well resolved and adjacent so that they could be fitted simultaneously. For p-wave resonances, which are much weaker, the intensity ratio between the doublet at 235.7-237.1 keV and the peak at 191.5 keV was calibrated. Spins were assigned to 55 s-wave resonances and 23 p-wave resonances, which are indicated in Tables 8 and 9, respectively.

A general tendency to populate more those  $^{110}\text{Ag}$  low-lying levels of parity opposite to that of the initial state was noticed. In Fig. 22 are plotted, for all resonances with  $J=1$ , the intensity ratios of the line at 198.7 keV, de-exciting a  $2^+$  state, and of the doublet at 235.7-237.1 keV, both de-exciting negative parity states; a clear-cut division between the two groups of s- and p-wave levels is visible, and the magnitude of the effect is comparable to the one related to the spin dependence. This effect has been exploited for assigning the parity of the resonances under consideration, also in the cases where other methods (like the Bayes test on conditional probabilities) give ambiguous results. However, this effect being reported for the first time deserves to be studied on its own merit, since it can yield information on the mechanism of radiative capture. Therefore these investigations will be pursued in two directions: first, by searching for the effect in other nuclides; second, by trying to reproduce it in simulations of the gamma decay.

**Table 8. Spin assignment for 55 s-wave resonances in  $^{109}\text{Ag}$**

$E_0(\text{eV})$	$J^a$	$J^b$												
30.4	1	1	259.0	0		469.7	0	0	747.6	1		1009	0	
40.1	1	1	272.6	1		488.0	1		784.7	1		1037	1	
55.7	0	0	291.0	1	0	500.6	1	1	803.8	1		1057	1	
70.8	1	1	300.9	0		512.6	0	0	848.5	1		1062	0	
87.7	1	1	316.5	1	1	557.2	1		861.8	1		1116	1	
106.3	0		327.8	1		560.7	0	0	883.0	1		1204	1	
133.9	1	1	360.4	1		565.5	1	1	902.8	1		1219	1	
139.7	1	0	387.0	1	1	608.1	1	1	933.0	1		1236	1	
173.1	1	1	398.0	1	1	622.4	1	0	949.3	1		1254	1	
209.6	1	1	404.4	0	0	669.5	1		961.0	0		1300	1	
251.3	1	1	428.6	1		726.1	1		976.0	1		1383	0	

<sup>a</sup> present work; <sup>b</sup> Mughabghad et al., Neutron Cross Sections, Academic Press (1981)

Table 9. Spin assignment for 23 p-wave resonances in  $^{109}\text{Ag}$

$E_0(\text{eV})$	J								
32.7	1	164.4	2	284.3	2	391.6	1	690.5	0
82.4	2	169.8	0	293.3	1	441.0	1	821.5	2
91.5	2	199.0	1	340.2	2	446.5	2	831.4	2
113.5	2	218.0	2	351.4	2	526.7	1		
160.2	1	264.7	2	374.5	2	681.5	2		

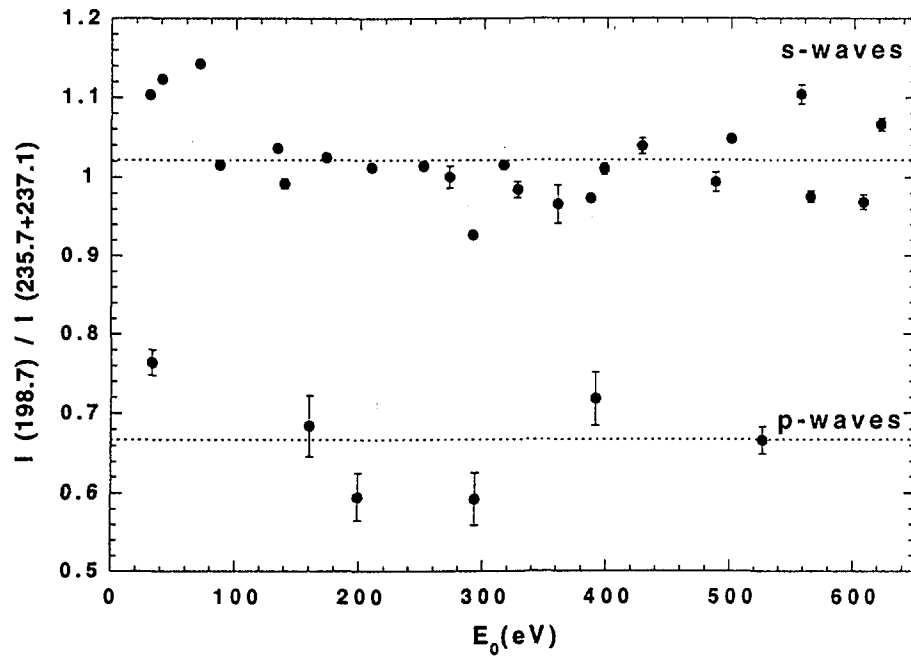


Fig. 22. Intensity ratios for  $J=1$  resonances

## NUCLEAR DATA FOR FUSION TECHNOLOGY

The objective of the work on nuclear data for fusion technology is to contribute to an improved knowledge of data for neutron transport calculation in the blanket and for an estimate of the gas production. Measurements are presently done for high resolution inelastic scattering cross sections and cross sections for (neutron, charged particle) reactions. The work on neutron inelastic scattering from  $^{56}\text{Fe}$  has been described in the chapter "Nuclear Data for Fission Technology" as it is relevant to both areas.

### *Isomeric Cross Section Ratios for the Formation of $^{53\text{m,g}}\text{Fe}$ and $^{52\text{m,g}}\text{Mn}$ in Fast Neutron-Induced Reactions on $^{54}\text{Fe}$*

A. Fessler\*, S. M. Qaim\*\*, E. Wattecamp

The isomeric cross section ratio  $\sigma_m/(\sigma_m+\sigma_g)$  for the formation of  $^{53\text{m,g}}\text{Fe}$  and  $^{52\text{m,g}}\text{Mn}$  in  $^{54}\text{Fe}(n,2n)$  and  $^{54}\text{Fe}(n,t)$  reactions, respectively, was measured at the IRMM 7 MV Van de Graaff accelerator in the neutron energy range from 18 to 21 MeV. Samples of natural isotopic composition (pressed pellets of iron powder) or enriched  $\text{Fe}_2\text{O}_3$  were used.

The neutrons were produced via the (d,t) reaction on a Ti/T-target. The duration of the irradiations varied from some minutes to some days, depending on the half life of the activation product. Use was made of the activation technique in combination with high-resolution  $\gamma$ -ray spectrometry. In the work on  $^{53\text{m,g}}\text{Fe}$  only relative measurements were carried out (i.e. no neutron flux density was determined) since the metastable state ( $J^\pi = 19/2^-$ ,  $E_x = 3.041\text{MeV}$ ) decays with 100% IT to the ground state ( $J^\pi = 7/2^-$ ). In case of the formation of  $^{52\text{m,g}}\text{Mn}$  two independent cross section measurements were performed for the metastable ( $J^\pi = 2^+$ ,  $E_x = 0.378\text{ MeV}$ ) and the ground state ( $J^\pi = 6^+$ ), (see Fig. 23). The isomeric cross section ratios for the formation of  $^{53\text{m,g}}\text{Fe}$  are shown in Fig.24 together with a model calculation performed with the code STAPRE-H95<sup>(1)</sup> Experiment and calculation agree quite well. The ratio is about a factor of ten smaller compared to recent measurements with the  $^{52}\text{Cr}(^3\text{He},2n)^{53\text{m,g}}\text{Fe}$  reaction<sup>(2)</sup>. It seems that the mass and charge of the projectile have some effect on the formation of the metastable state.

The isomeric cross section ratio for the formation of  $^{52\text{m,g}}\text{Mn}$  (see Fig. 25) shows a similar behaviour compared to the formation in the  $^{52}\text{Cr}(^3\text{He},t+dn+p2n)^{52\text{m,g}}\text{Mn}$

\* EC Fellow from Forschungszentrum Jülich GmbH, Germany

\*\* Forschungszentrum Jülich GmbH, Germany

(1) M. Avrigeanu, M. Ivascu, V. Avrigeanu, NEA Data Bank, IAEA 0971/03 (1995)

(2) A. Fessler, S. M. Qaim, Rad. Acta **72**, 121 (1996)

reactions<sup>(3)</sup>. Here no significant influence of the mass and charge of the projectile can be observed. Further measurements have to be done with other projectiles (p, d,  $^4\text{He}$ , ...), in order to obtain more information about these findings.

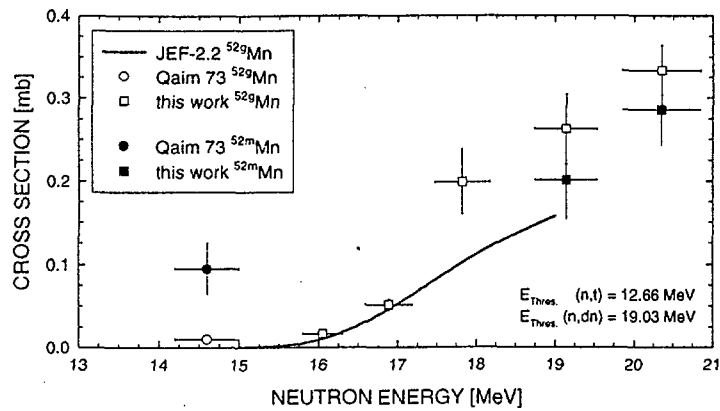


Fig. 23. Cross sections for the  $^{54}\text{Fe}(n,t+dn)^{52m}\text{Mn}$  and  $^{54}\text{Fe}(n,t+dn)^{52g}\text{Mn}$  reactions

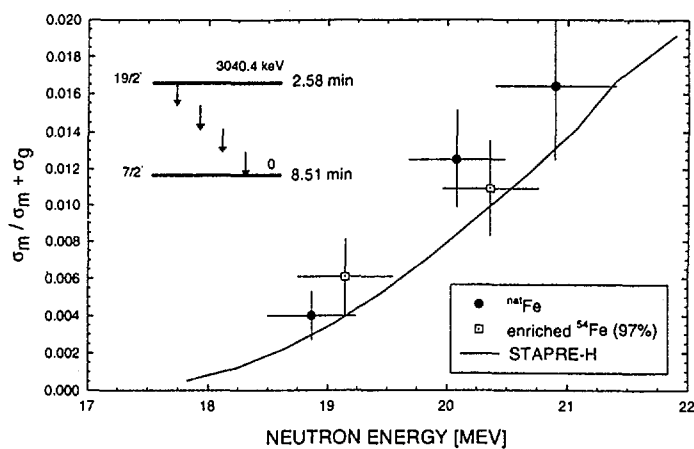
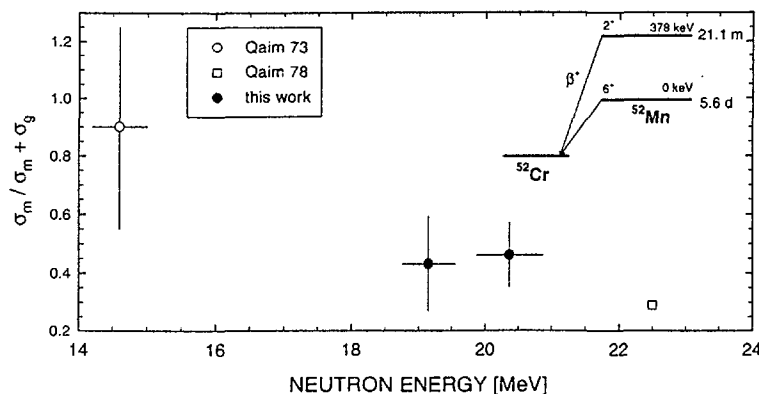


Fig. 24. Isomeric cross section ratio for the  $^{54}\text{Fe}(n,2n)^{53m,g}\text{Fe}$  reaction

<sup>(3)</sup> A. Fessler, Diploma Thesis, University of Köln (1994).



**Fig. 25. Isomeric cross section ratio for the  $^{54}\text{Fe}(n,t+dn)^{52m,g}\text{Mn}$  reaction**  
 (the point at 22.5 MeV was measured in a neutron spectrum produced via break-up  
 of 53 MeV deuterons on Be ( $E_n=11.5\text{-}43.5$  MeV;  $I_{\text{max}}$  at 22.5 MeV; FWHM = 15.8 MeV)

### Neutron Activation Cross Sections in the Energy Range 16 - 20 MeV

A. Fessler\*, Y. Ikeda\*\*, S. M. Qaim\*\*\*, D. L. Smith\*\*\*\*, E. Wattecamps

A new collaboration started with KFA (Germany), ANL (USA) and JAERI-Tokai (Japan) with special interest in short-lived isotopes. The irradiations have been carried out at the 7 MV Van de Graaff accelerator for five neutron energies in the range 16 - 20 MeV using the  $\text{T}(d,n)^4\text{He}$  source reaction. The activities observed have half lives ranging from 7 seconds to several hours, but most were from about 30 seconds to a few minutes. A pneumatic sample transport system was built. The induced radioactivities were measured by observing  $\gamma$ -rays emitted from the irradiated samples with a germanium detector.

Samples of natural isotopic composition as well as enriched isotopes were used. Most of the enriched isotopes were made available by JAERI. The natural samples and some of the enriched ones were prepared by the Nuclear Samples Preparation Group. Table 10 gives an overview of the investigated reactions. The reference cross sections were those of the  $^{27}\text{Al}(n,p)^{27}\text{Mg}$ ,  $^{27}\text{Al}(n,\alpha)^{24}\text{Na}$  and  $^{93}\text{Nb}(n,2n)^{92m}\text{Nb}$  reactions. For some of the investigated reactions nuclear model calculations have been started with the code STAPRE-H95. Measurements for long-living isotopes ( $T_{1/2}$  of several hundred days to some years) are planned.

\* EC Fellow from Forschungszentrum Jülich GmbH

\*\* JAERI-Tokai, Japan

\*\*\* Forschungszentrum Jülich GmbH

\*\*\*\* Visiting Scientist from ANL, USA

As by-product from the cross section measurement program the half life of  $^{53}\text{V}$  was determined. The measured the radioactivity of  $^{53}\text{V}$  was produced via the  $^{53}\text{Cr}(n,p)^{53}\text{V}$  and  $^{54}\text{Cr}(n,np)^{53}\text{V}$  reactions by the irradiation of an elemental chromium metal sample with fast neutrons.

**Table 10. List of the investigated neutron activation reactions (  requested by WPEC, subgroup C)**

Reaction	$T_{1/2}$ of Product*	Sample	Status**
$^{11}\text{B}(n,p)^{11}\text{Be}$	13.81(8) s	$^{\text{nat}}\text{B}$	3
$^{16}\text{O}(n,2n)^{15}\text{O}$	122.24(16) s	$\text{MnO}_2$	3
$^{16}\text{O}(n,p)^{16}\text{N}$	7.13(2) s	$\text{MnO}_2$	3
$^{19}\text{F}(n,p)^{19}\text{O}$	26.91(8) s	Teflon	3
$^{23}\text{Na}(n,p)^{23}\text{Ne}$	37.24(12) s	$\text{NaCl}$	2
$^{23}\text{Na}(n,\alpha)^{20}\text{F}$	11.00(2) s	$\text{NaCl}$	2
$^{25}\text{Mg}(n,p)^{25}\text{Na}$	59.1(6) s	enr. $^{25}\text{MgO}$ (98.8%)	2
$^{28}\text{Si}(n,p)^{28}\text{Al}$	2.2414(12) m	$\text{SiO}_2$	2
$^{29}\text{Si}(n,p)^{29}\text{Al}$	6.56(6) m	enr. $^{29}\text{SiO}_2$ (95.1%)	2
$^{31}\text{P}(n,\alpha)^{28}\text{Al}$	2.2414(12) m	$^{\text{nat}}\text{P}$	2
$^{37}\text{Cl}(n,p)^{37}\text{S}$	5.05(2) m	$\text{NaCl}$	2
$^{35}\text{Cl}(n,2n)^{34\text{m}}\text{Cl}$	32.00(4) m	$\text{NaCl}$	2
$^{46}\text{Ti}(n,p)^{46\text{m}}\text{Sc}$	18.75(4) s	enr. $^{46}\text{TiO}_2$ (81.2%)	2
$^{50}\text{Ti}(n,p)^{50}\text{Sc}$	102.5(5) s	enr. $^{50}\text{TiO}_2$ (96.8%)	2
$^{51}\text{V}(n,p)^{51}\text{Ti}$	5.76(1) m	$^{\text{nat}}\text{V}$	2
$^{50}\text{Cr}(n,np)^{49}\text{V}$	330(15) d	$^{\text{nat}}\text{Cr}$	4
$^{52}\text{Cr}(n,p)^{52}\text{V}$	3.75(1) m	$^{\text{nat}}\text{Cr}$ , enr. $^{52}\text{Cr}_2\text{O}_3$ (99%)	1
$^{53}\text{Cr}(n,np)^{52}\text{V}$	3.75(1) m	enr. $^{53}\text{Cr}_2\text{O}_3$ (98%)	2
$^{53}\text{Cr}(n,p)^{53}\text{V}$	1.61(4) m	$^{\text{nat}}\text{Cr}$ , enr. $^{53}\text{Cr}_2\text{O}_3$ (98%)	1
$^{54}\text{Cr}(n,np)^{53}\text{V}$	1.61(4) m	enr. $^{54}\text{Cr}_2\text{O}_3$ (93%)	2
$^{54}\text{Cr}(n,p)^{54}\text{V}$	49.8(5) s	enr. $^{54}\text{Cr}_2\text{O}_3$ (93%)	2
$^{54}\text{Cr}(n,\alpha)^{51}\text{Ti}$	5.76(1) m	enr. $^{54}\text{Cr}_2\text{O}_3$ (93%)	2
$^{55}\text{Mn}(n,\alpha)^{52}\text{V}$	3.75(1) m	$\text{MnO}_2$	2
$^{54}\text{Fe}(n,2n)^{53}\text{Fe}$	8.51(2) m	$^{\text{nat}}\text{Fe}$ , enr. $^{54}\text{Fe}_2\text{O}_3$ (97%)	2
$^{54}\text{Fe}(n,t)^{52\text{m}}\text{Mn}$	21.1(2) m	enr. $^{54}\text{Fe}_2\text{O}_3$ (97%)	2
$^{54}\text{Fe}(n,t)^{52\text{g}}\text{Mn}$	5.591(3) d	$^{\text{nat}}\text{Fe}$	2
$^{57}\text{Fe}(n,p)^{57}\text{Mn}$	87.2(8) s	enr. $^{57}\text{Fe}$	2
$^{57}\text{Fe}(n,np)^{56}\text{Mn}$	2.5785(2) h	enr. $^{57}\text{Fe}$	2
$^{58}\text{Ni}(n,\alpha)^{55}\text{Fe}$	2.73(3) y	$^{\text{nat}}\text{Ni}$	4
$^{62}\text{Ni}(n,p)^{62\text{m}}\text{Co}$	13.91(5) m	enr. $^{62}\text{Ni}$	2
$^{62}\text{Ni}(n,p)^{62\text{g}}\text{Co}$	1.50(4) m	enr. $^{62}\text{Ni}$	2
$^{119}\text{Sn}(n,p)^{119}\text{In}$	2.4(1) m	enr. $^{119}\text{SnO}_2$ (84.5%)	2
$^{138}\text{Ba}(n,2n)^{137\text{m}}\text{Ba}$	2.552(1) m	enr. $^{138}\text{BaCO}_3$ (99.7%)	2

\* R. B. Firestone, Table of Isotopes, 8<sup>th</sup> Edition, Wiley & Sons (1996)

\*\*

- 1 Irradiations done, data analysis finished
- 2 Irradiations done, data analysis in progress
- 3 Additional irradiations have to be performed
- 4 Irradiations are planned

## NUCLEAR METROLOGY

### RADIONUCLIDE METROLOGY

The objective of the work on radionuclide metrology is to advance the experimental know-how in the field of radioactivity. This is done in four major areas: the determination of decay-scheme data, the improvement and development of measurement techniques, the preparation of particular standard and reference samples and the participation in international comparisons and evaluations.

#### *Preparation and Distribution of a Solution for the BIPM Comparison of $^{192}\text{Ir}$ Activity Measurements*

D.F.G. Reher, G. Sibbens, T. Altzitzoglou, B. Denecke

BIPM organises about one international comparison of activity measurements per year. The selection of the radionuclide is done at the bi-annual meetings of CCEMRI(II). Before a large scale comparison is launched, a trial comparison among the most experienced laboratories is organised.

At the 13<sup>th</sup> meeting of the CCEMRI(II) it was decided to launch a trial comparison of activity measurements of  $^{192}\text{Ir}$ . The reasons for the choice were that  $^{192}\text{Ir}$  is the most used radionuclide in radiotherapy, and that the results of the international reference system (SIR) at BIPM show still a systematic discrepancy of 1.5% between two distinct groups of results. IRMM had been selected to prepare a reference solution for distribution to 11 participating standards laboratories world-wide.

A commercial  $^{192}\text{Ir}$  solution was diluted with HCl. The carrier in the solution was about 5 mg of iridium per ml of solution in the form of  $\text{Na}_2\text{IrCl}_6$ . Samples of the solutions were analysed for radionuclide impurities by  $\gamma$ -ray spectrometry; no impurities were detected. After homogenisation 15 SIR-standard ampoules were filled with 3.6 g of solution and sealed. The mass of the solution in each ampoule was weighed to better than  $\pm 0.01\%$ . Before distribution to the participating laboratories (NPL, OMH, BIPM, VNIM, KRISS, ETL, IRA, LPRI, IIR and IRMM) the ampoules were measured repeatedly in the IRMM secondary standard ionisation chamber. Ampoules sent to the participants had a deviation from the average value of all ampoules of less or equal to  $\pm 0.02\%$ .

*Standardisation of a  $^{192}\text{Ir}$  solution in the frame of the BIPM trial comparison*

D.F.G. Reher, G. Sibbens, B. Denecke, T. Altzitzoglou

IRMM participated in the BIPM trial comparison of activity measurements of a solution of  $^{192}\text{Ir}$  using four independent methods: (1)  $4\pi\beta\text{-}\gamma$ -coincidence counting, (2)  $4\pi\gamma$ -counting (6''x6'' NaI(Tl)-well), (3)  $4\pi\beta\gamma$ -counting ( $4\pi\text{CsI(Tl)}$ ) and (4)  $4\pi\beta\gamma$ -sum counting (6''x6'' NaI(Tl)-well + pressurised proportional counter).

Dilutions were made and sources prepared from ampoule Nr. 9616. The masses of the sources were determined to an accuracy of  $\pm 0.1\%$  using a Mettler AT21 balance and a calibrated weighing set. In the same order of magnitude were the uncertainties for counting statistics, dead time, timing and radioactive decay. In Table 11 the results are given.

*Table 11. IRMM results of the  $^{192}\text{Ir}$  trial comparison. The uncertainties are given at the level of one standard deviation*

Method	Result (MBq/g)	Uncertainty (%)	Main unc. contrib. due to
$4\pi\beta\text{-}\gamma$ -coincidence counting	$1.093 \pm 0.003$	0.3	efficiency extrapolation
$4\pi\gamma$ -counting(6''x6'' NaI(Tl)-well)	$1.086 \pm 0.004$	0.4	efficiency extrapol. to zero energy
$4\pi\beta\gamma$ -counting ( $4\pi\text{CsI(Tl)}$ )	$1.088 \pm 0.004$	0.4	extrapol. to zero energy, dilution
$4\pi\beta\gamma$ -sum counting (6''x6'' NaI(Tl)-well + pr. pr. cntr.)	$1.099 \pm 0.007$	0.6	total efficiency timing
<b>Weighted Average</b>	<b><math>1.090 \pm 0.004</math></b>	<b>0.4</b>	
Ionisation chamber	$1.089 \pm 0.004$	0.4	calibration from earlier comparisons

The results of the three first methods agree rather well,  $4\pi\beta\gamma$ -sum counting, gives a higher result. The reason for this is that non optimum timing between the  $\beta$  and  $\gamma$  channels always leads to a higher result. Additionally, this method is new at IRMM and only one source was measured.

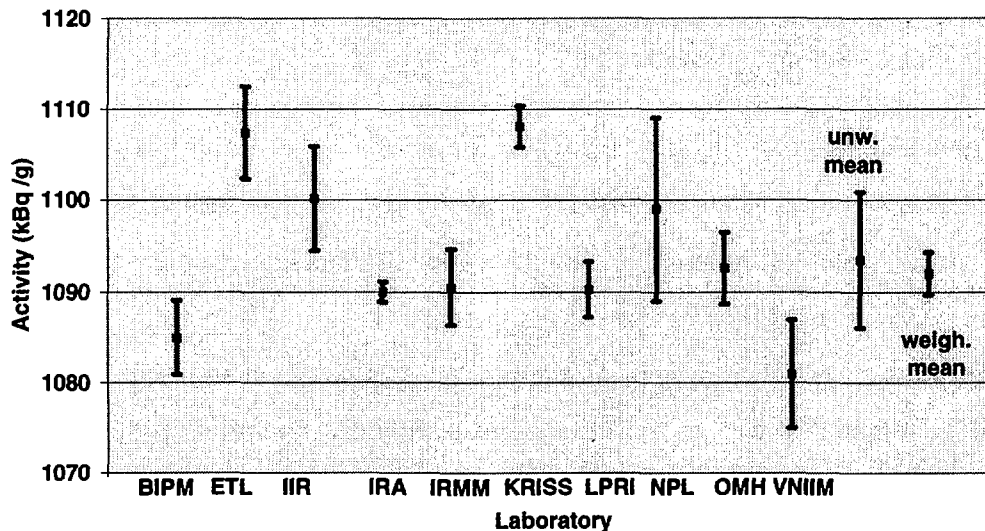
Results of the BIPM trial comparison of  $^{192}\text{Ir}$  activity standardisation

Fig. 26. Results of the BIPM  $^{192}\text{Ir}$  trial comparison

The result of the comparison is shown in Fig. 26. The spread of 2.5% is rather high and so is the standard deviation of  $\pm 0.7\%$ . It is clear that the problem in standardising  $^{192}\text{Ir}$  solutions is not yet solved. Very probably, a new trial comparison will be necessary before a world-wide large comparison can be launched.

### Low-Energy X-Ray Measurements and Standards

B. Denecke, G. Grosse

The standardisation work for low-energy X-ray sources was continued. For the investigation of nuclear processes in stars three  $^{37}\text{Ar}$  samples were standardised for their number of Ar atoms. A stability test of these ion-implanted samples showed no loss of Ar from the supporting aluminium foil.

Two standardised KX-ray fluorescence-source sets were sold to external customers. They were delivered in a special storage box together with the source handling tools and step by step assembling instructions. Both sets were measured in the windowless Si(Li) spectrometer to establish a calibration of this spectrometer. The production of new  $^{55}\text{Fe}$  excitation sources had to be delayed due to the closure of the radioactivity handling facilities.

Several users of low-energy X rays will join the planned EUROMET project on "Establishment of low-energy photon standards". IRMM has accepted to act as coordinator for this project.

### ***High Pressure Proportional Gas Counter***

B. Denecke, G. Grosse, T. Szabo

The pressurised  $4\pi$ -proportional gas counter for the  $4\pi$ -Auger- $\gamma$  coincidence counter was revised and assembled. The pressure vessel of the counter was successfully tested at 45 bar. No irreversible deformation of the thin-walled Al container was found. The counter was operated with a gas flow at open atmosphere.

The high-pressure gas-flow system for the counter was designed and built into a compact frame. The emphasis was to construct a user-friendly operation panel to minimise handling errors, which may destroy parts of the equipment. The aim was to establish a counting-gas flow with a constant gas density in the counter which is needed for a stable energy threshold. This was achieved by controlling the pressure of the gas flow to be equal to the pressure in a small reference pressure vessel placed near the counter inside the same lead shield. Basically, it consists of a two-stage back-pressure regulation system. Nearly all the commercially available parts of the equipment were modified to meet the requirements of this precision gas-flow system. The gas-flow control valve, which must handle only part of the gas flow of a few  $\text{cm}^3 \text{min}^{-1}$ , was a complete new design and is performing well. It is based on the dilatation of a stack of low-voltage piezo crystals by only some  $\mu\text{m}$ .

### ***Standardisation of $^{63}\text{Ni}$ and $^{55}\text{Fe}$ Solutions by Liquid Scintillation Counting***

T. Altzitzoglou

The standardisation of  $^{63}\text{Ni}$  and  $^{55}\text{Fe}$  solutions was done in the framework of the EUROMET 297 action, using the Liquid Scintillation Counting (LSC) technique. The purpose was to compare activity measurement methods in LSC, and in particular the CIEMAT/NIST method<sup>(1)</sup> and the Triple-to-Double Coincidence Ratio (TDCR) method and to exchange calculation models and ideas on the topic.

The action started in 1994 with the standardisation of  $^{63}\text{Ni}$ . The results were inconclusive, mostly because the  $^{63}\text{Ni}$  solution gave unstable sources in the Ultima Gold<sup>®</sup> liquid scintillation cocktail. It was then decided to repeat the  $^{63}\text{Ni}$  standardisation together with the standardisation of the  $^{55}\text{Fe}$  solution, both provided by the Laboratoire Primaire des Rayonnements Ionisants (LPRI, Gif-sur-Yvette, France).

---

<sup>(1)</sup> E. Garcia-Toraño and A. Grau Malonda, *Comp. Phys. Comm.* 36 (1985) 307

Eleven laboratories world-wide participated in the standardisation of  $^{63}\text{Ni}$ , a pure  $\beta$  emitter with a 66 keV maximum decay energy. Activity concentration measurements of  $^{63}\text{Ni}$  samples, prepared gravimetrically at IRMM, were performed using a commercial two-phototube liquid scintillation counter. In total 24 samples of  $^{63}\text{Ni}$ , with varying degrees of chemical quenching, were measured more than 12 times each over a period of 45 days. The stability of the sources was very good. In addition,  $^3\text{H}$  samples prepared from an IRMM  $^3\text{H}$  standard solution were measured. The analysis of the data was done by both the CIEMAT/NIST method and the Efficiency Tracing method<sup>(1)</sup>. In the first method, the efficiency of the LSC for  $^{63}\text{Ni}$  was calculated by the program EFFY4<sup>(1)</sup>. For both methods, special computer programs were written for data reduction and analysis.

The results for the activity concentration of the  $^{63}\text{Ni}$  solution from the eleven participating laboratories are shown in Fig. 27. The IRMM result is  $(40.1 \pm 0.2)$  kBq/g on 1/1/96 0h UT and the mean value of all laboratories is  $39.97 \pm 0.26$  kBq/g on the same reference date. The final conclusion is that the CIEMAT/NIST and TDCR methods give very similar results for the activity concentration of the  $^{63}\text{Ni}$  solution.

Liquid scintillation counting is a relatively easy method for the standardisation of  $^{55}\text{Fe}$ , which decays by electron capture and emits low energy electrons and X-rays (about 5 keV). Ten laboratories from all over the world participated in this standardisation.

In total 24 samples of  $^{55}\text{Fe}$  in Ultima Gold<sup>®</sup> and 10 samples in Insta Gel<sup>®</sup>, with varying degrees of chemical quenching, were prepared gravimetrically and measured more than 12 times each over a period of 35 days. The stability of the sources in Ultima Gold<sup>®</sup> was poor, in contrast to those prepared in Insta Gel<sup>®</sup>.

The analysis of the data was done by the CIEMAT/NIST method; the efficiency of the LSC for  $^{55}\text{Fe}$  was calculated with the program EMI. Special computer programs were written for data reduction and analysis.

The results for the activity concentration of the  $^{55}\text{Fe}$  solution from all participating laboratories are shown in Fig. 28. The IRMM result is  $(50.2 \pm 0.4)$  kBq/g on 1/1/96 0h UT for the samples in Ultima Gold<sup>®</sup> and  $(53.1 \pm 0.3)$  kBq/g for the samples in Insta Gel<sup>®</sup>. The mean value of all laboratories is  $(51.05 \pm 1.65)$  kBq/g on the same reference date. The conclusion is that the dispersion between the activity concentration of the  $^{55}\text{Fe}$  solution measured by the ten laboratories is quite high (about 3%), but there is no obvious

---

<sup>(1)</sup> H. Ishikawa, M. Takiue and T. Aburai, *Int. J. Appl. Radiat. Isot.* 35 (1984) 463

correlation between the results and the measurement methods. However, there is correlation between the results and the scintillator cocktails used.

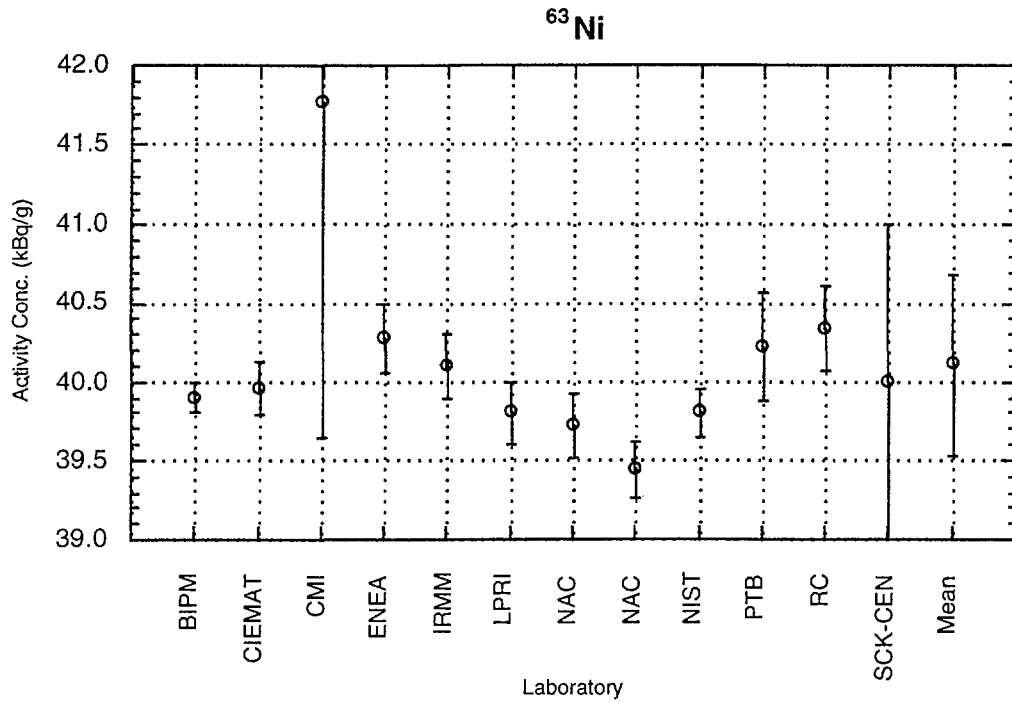


Fig. 27.  $^{63}\text{Ni}$  EUROMET 297 activity concentration results, given in kBq/g on 1/1/96 0h UT

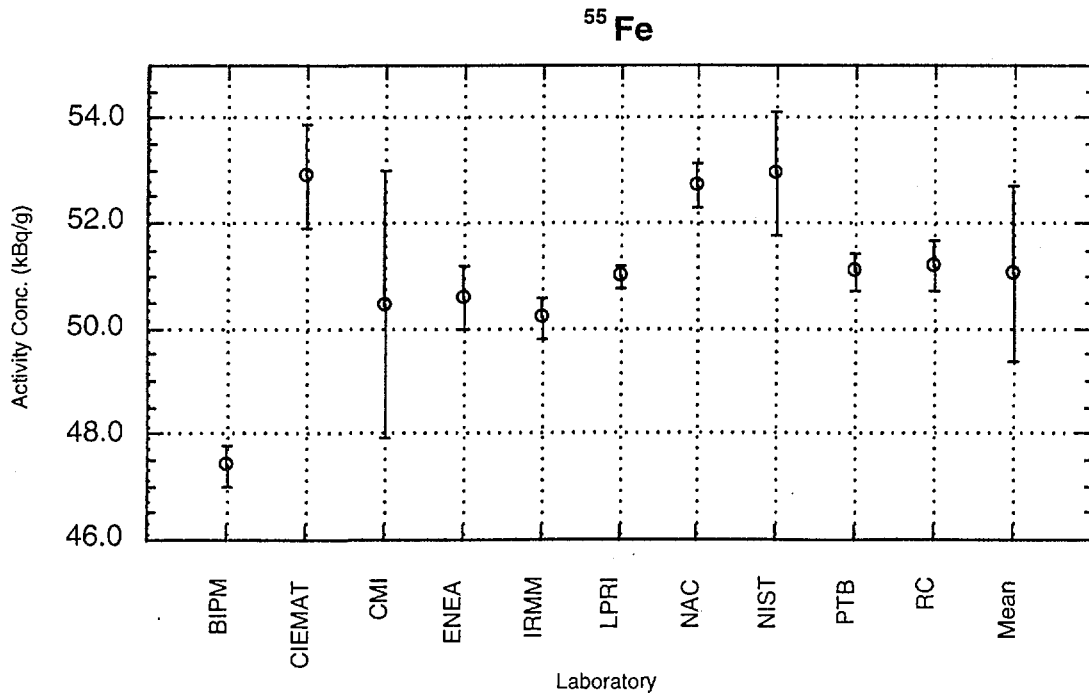


Fig. 28.  $^{55}\text{Fe}$  EUROMET 297 activity concentration results, given in kBq/g on 1/1/96 0h UT

***Radiochemical Intercomparison of the NIST Bone Ash SRM***

T. Altzitzoglou (co-ordinator), M. Bickel, J.J. LaRosa\*, D. Mouchel, C. Nicholl, R. Pilviö, R. Wordel

In the frame of a radiochemical intercomparison, five samples of the future NIST bone ash reference material (NIST SRM-4356) were analysed. The bone ash sample consists of 4.33 wt% actinides-contaminated human bone ash and 95.67 % diluent bovine bone ash.

Although it was a radiochemical exercise, first a non-destructive gamma-ray measurement of the samples was carried out, using low-background solid state photon detectors at the underground facility HADES. The samples after drying in an oven, were placed in special airtight Teflon containers and measured starting after equilibrium in the  $^{226}\text{Ra}$  decay chain was reached. These measurements provided the activity concentration of the  $^{241}\text{Am}$ ,  $^{210}\text{Pb}$ ,  $^{226}\text{Ra}$  and  $^{228}\text{Th}$  nuclides, as well as a first check of the homogeneity of the lot.

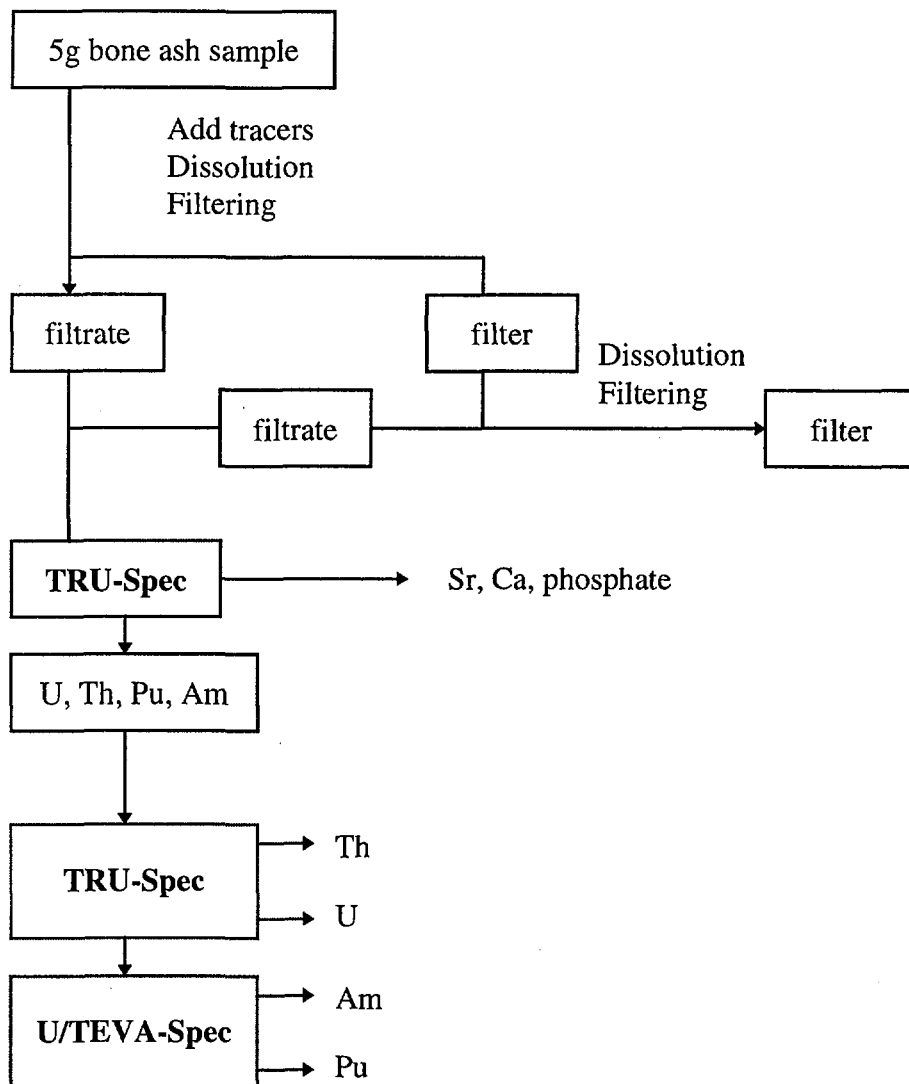
The work continued with the radiochemical destructive analysis which included the addition of radiochemical tracers, the dissolution of the samples, the chemical chromatographic separation and isolation of the elements of interest and the measurement by appropriate methods (e.g. liquid scintillation counting for  $^{90}\text{Sr}$ , alpha spectrometry for  $^{234}\text{U}$ ,  $^{238}\text{U}$ ,  $^{238}\text{Pu}$ ,  $^{239,240}\text{Pu}$ ,  $^{241}\text{Am}$ ,  $^{228}\text{Th}$ ,  $^{230}\text{Th}$  and  $^{232}\text{Th}$ ). A radiochemical procedure was developed to separate strontium and the actinides based on extraction chromatography using a crown ether (Eichrom Ind., Inc.).

No radioactive strontium was added as tracer to avoid interference during counting. Instead, natural strontium was added as carrier and the chemical recovery was determined gravimetrically. The natural strontium content of the bone ash itself was determined by ICP-MS and the appropriate correction to the chemical recovery of strontium was applied. In Figs. 29 and 30 the simplified chemical separation schemes for the strontium and the actinides, respectively, are shown. The chemical separations, the measurements and the analysis of the data have been terminated and the final results have been dispatched to NPL, the European co-ordinator of this exercise.

---

\* Visiting Scientist from IAEA

**Separation scheme of actinides from bone ash samples**



Coprecipitation with  $\text{NdF}_3$  and electrodeposition in ammonium sulfate medium were used as sample preparation methods for alpha spectrometry.

*Fig. 29. Simplified separation scheme of actinides from bone ash samples*

**Separation scheme of strontium from bone ash samples**

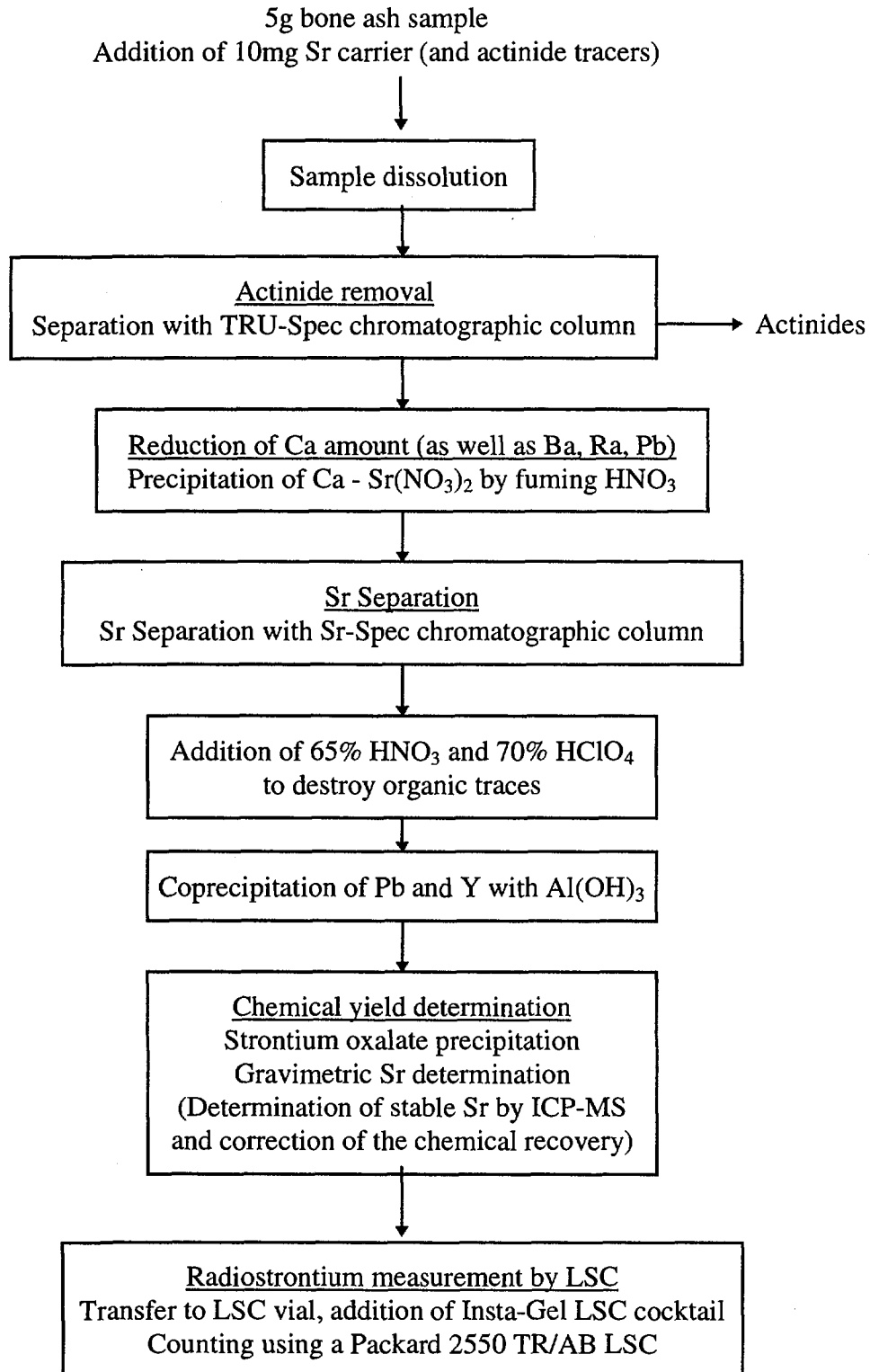


*Fig. 30. Simplified separation scheme of strontium from bone ash samples*

### ***Standardisation of $^{90}\text{Sr}$ and $^{90}\text{Y}$ by Liquid Scintillation Counting***

T. Altitzoglou

With the increasing interest in environmental samples, the measurement of  $^{90}\text{Sr}$  attracts considerable attention.  $^{90}\text{Sr}$  is a pure beta emitter and it is necessary to use radiochemical separation prior to counting. A procedure for the  $^{90}\text{Sr}$  and  $^{90}\text{Y}$  standardisation and activity measurement by Liquid Scintillation Counting (LSC), based on a full spectrum dual label technique is under development. The method does not require that the two nuclides are in equilibrium. Combined with the CIEMAT/NIST efficiency tracing method,  $^{90}\text{Sr}$  and  $^{90}\text{Y}$  standards are not needed. Instead, a set of  $^3\text{H}$  standards and qualitative sets of  $^{90}\text{Sr}$  and  $^{90}\text{Y}$  with varying degree of quenching are required. The procedure can equally be applied to other suitable pairs of radionuclides and be extended to more nuclides in the sample.

### ***Euromet Project Nr. 325 on the Analysis of Plutonium Alpha-particle Spectra***

G. Bortels, A. Verbruggen, G. Sibbens, T. Altitzoglou

The aim of the intercomparison was to establish the state of the practice for analysing  $^{238,239,240}\text{Pu}$  alpha-particle spectra<sup>(1)</sup>.

Two types of plutonium sources were prepared at IRMM: vacuum-evaporated sources and drop-deposited sources. They were measured at IRMM and the spectra were sent to eight laboratories. Participants had to determine the  $^{239}\text{Pu}/^{240}\text{Pu}$  and the  $^{238}\text{Pu}/^{239+240}\text{Pu}$  activity ratios by analysing the spectra.

The results reveal that using vacuum-evaporated sources, measurements of  $^{239}\text{Pu}/^{240}\text{Pu}$  activity ratios have been achieved within 1%. The results of the drop-deposited source spectra show more spread due to the increased tailing and larger FWHM of the peaks.

### ***Low-activity Lead Investigated by Low Background HPGe $\gamma$ -Ray Spectrometry in an Underground Laboratory, $\beta$ -Spectrometry and Calorimetry***

R. Wordel, D. Mouchel, C. Ingelbrecht, F. Peetermans, D. Arnold\*, H. Wershofen\*, V.A. Sole\*\*, J. Höhne\*\*\*, M.L. Sarsa\*\*\*, J. Schnagel\*\*\*, E. Kellner\*\*\*, F. v. Feilitzsch\*\*\*

Selection of low activity lead used to shield low-level detectors was done with a low-energy low-level Ge detector in an underground laboratory, with calorimetry or with

<sup>(1)</sup> G. Bortels, A. Verbruggen, G. Sibbens, T. Altitzoglou, Internal Report IRMM GE/R/RN/01/96

\* Physikalisch Technische Bundesanstalt, Germany

\*\* European Molecular Biology Laboratory, Germany

\*\*\* Physik Department, Technische Universität München, Germany

$\beta$ -spectrometry. The detection limit for  $\beta$  counting is about  $3 \text{ Bq kg}^{-1}$ , about  $0.5 \text{ Bq kg}^{-1}$  for underground  $\gamma$ -ray spectrometry and  $0.02 \text{ Bq kg}^{-1}$  for calorimetry without special shielding. Only  $^{210}\text{Pb}$  and its daughters  $^{210}\text{Bi}$  and  $^{210}\text{Po}$  are responsible for the intrinsic radioactivity of lead. The very soft  $\beta^-$  ( $E_{\text{max}}$  of 16.5 and 63 keV) radiation of  $^{210}\text{Pb}$  hardly escapes from the bulk material and the 46.5 keV  $\gamma$  radiation allows to investigate just a limited volume at the surface of the sample (self-absorption length 0.06 mm). A larger volume is accessible due to the energetic (1.16 MeV)  $\beta$  rays of  $^{210}\text{Bi}$ . They induce bremsstrahlung and characteristic X rays in lead. The bremsstrahlungs continuum has its maximum at about 170 keV while the lead X rays have energies of 72.8, 75.0, 84.9 and 87.4 keV. Calorimetry is able to investigate the entire bulk of the sample and is therefore the most sensitive method. Modern commercial lead, labelled as low-level lead, and ancient lead samples have been measured. They originated from old French monuments and from Hampton Court (Great Britain) and one being of Etruscan origin, at least 2200 years old. As the reference, a lead disk was used having an activity of  $70.1 \text{ Bq}\cdot\text{kg}^{-1}$ , determined radiochemically. Results are between  $< 0.02 \text{ Bq}\cdot\text{kg}^{-1}$  (Etruscan lead) and  $700 \text{ Bq kg}^{-1}$  for a commercial lead. Non-selected lead can have more than  $1000 \text{ Bq kg}^{-1} \text{ }^{210}\text{Pb}$  (Table 12).

**Table 12.** Activity concentration of  $^{210}\text{Pb}$ ,  $\text{Bq kg}^{-1}$ , in lead samples

a	b	c	d	e	f	g	h	i
$29 \pm 3$	$8 \pm 2$	$230 \pm 12$	$293 \pm 15$	$693 \pm 32$	$14 \pm 2$	$2.4 \pm 1.3$	$< 1$	$70.1 \pm 1.4$

a, b, c, d, selected, commercial available lead batches; e ordinary lead; f, g, ancient lead from English and French monuments, used in our shieldings; h Etruscan sample; i reference sample from PTB.

### ***IRMM Low Level Underground Laboratory in HADES***

D. Mouchel, R. Wordel

The equipment of the underground laboratory has been completed. In particular, two new shieldings have been designed with low radioactivity materials, old lead and special copper selected by own means (Table 13).

**Table 13. HPGe detectors operated at HADES and the main specifications of their shieldings**

Ge volume [cm <sup>3</sup> ]	Relative efficiency (%)	Shielding material and thickness [cm]					Background counts s <sup>-1</sup> [5-2700]keV
		<u>electrolytic copper</u>	<u>lead</u>	<sup>210</sup> Pb activity [Bq kg <sup>-1</sup> ]	<u>lead</u>	<sup>210</sup> Pb activity [Bq kg <sup>-1</sup> ]	
100 coaxial	20	6	5 <sup>a</sup>	1	10 <sup>b</sup>	17	0.00666 <sub>6</sub>
40 semiplanar		6	10 <sup>a</sup>	1	5 <sup>c</sup>	700	0.00361 <sub>4</sub>
250 coaxial	60	15 <sup>d</sup>			14 <sup>e</sup>	15	

<sup>a</sup> lead originating from old French monuments, <sup>e</sup> from the Hampton Court roof, United Kingdom; <sup>b</sup> modern lead from the Bolinden company and <sup>c</sup> ordinary lead; <sup>d</sup> freshly produced copper, immediately stored underground to avoid the cosmogenic production of radionuclides, e.g. <sup>57</sup>, <sup>58</sup>, <sup>60</sup>Co. A fourth, modular shielding, planned to accommodate various types of experiments and built with copper <sup>d</sup> and lead <sup>e</sup> is available.

## TECHNICAL APPENDIX

### *Electron Linear Accelerator*

J-M. Salomé, M. Arias Arenas, K. Cairns, R. Cools, C. Díaz Vizoso, F. Melis, F. Menu, R. Van Bijlen, J. Waelbers

The linear accelerator was operated and used only for the neutron measurements programme. The electron beam was available during 3079 hours for these experiments. Neutrons are produced in a rotary uranium target via  $(\gamma, n)$  and  $(\gamma, f)$  reactions and moderated by water containing beryllium boxes. Twelve flight paths from 7 to 400 m long are equipped for neutron time-of-flight measurements. The electron beam is delivered according to the requested parameters. On the average 6.7 neutron beams are used simultaneously. Very short bursts of 1 to 2 ns are achieved by means of the post-acceleration compression magnet. After the Linac refurbishing, it was observed that the accelerator tuning to get these short pulses is very dependent on the water temperature of the bunching section. In view of keeping the compression quality we have to maintain the temperature regulation to  $\pm 0.1^\circ\text{C}$ .

For some high precision measurements, the position of the electron beam on the target had to be controlled. This is being realised by analysing the light produced by the electron beam on the target window.

New equipment to drive the large thyratrons was installed during the summertime. It consists of two tanks with power supplies, supporting circuitry and timing device connected through a fibre optic system. The working of these thyratrons operated up to 800 Hz at high power is drastically improved after this modification.

### *Van de Graaff Accelerators*

A. Crametz, M. Conti, W. Schubert, R. Thomas

The two Van de Graaff accelerators have been operated during 3397 hours; maintenance and improvement have requested 648 hours.

The accelerators have been operational as intensively as the years before (around 4000 hours) and no major modification has been performed this year. The radio-frequency (RF) ion source of the 7 MV has been replaced 4 times and one time for the 3.5 MV accelerator. During the second part of the year, the gas compressor which provides 1.6 MPa for the insulating gas inside the pressurised vessel was broken and will be repaired

beginning 1997, the beam energy was limited to 5.5 MeV. Due to water condensation on the cooling circuits during the hot period, the water cooling system has been split in two parts, one for the pressurised vessel at 10-12°C and a second one for components on beam lines and vacuum pumps at 18-20°C.

### ***Radiation Physics Laboratory***

M. Arias, A. Crametz, P. Henri\*, H. Riemenschneider, P. Rulhusen, J.-M. Salomé

The electron beamline outside of the neutron target hall has been installed. The target chamber, dipole bending magnet, and beam dump are in place. Installation of the heavy concrete shielding walls has been started. Two closed cooling water loops are also being installed, which will be connected to the cooling water for the compression magnet and for the photoactivation facility, respectively. All installation work is carried out during linac operation breaks. A new interlock system has been developed, based on a commercial computer controlled system. It integrates the accelerator hall, the neutron target hall, the target bunker and the radiation physics laboratory. It has been tested on a down scaled model and will be installed during the next larger linac shut down period.

### ***Analysis of B-C-N Coatings with NRA and BS Techniques***

G. Giorginis, A. Crametz, V. Garcia, M. Hult\*\*, L. Persson\*\*

The Prompt Charged Particle Activation Analysis (PCPAA) technique introduced at IRMM for the analysis of B-N coatings by using ( $\alpha,p$ ) reactions on boron and nitrogen<sup>(1)</sup> was extended to include carbon detection by elastic ( $\alpha,\alpha$ ) non-Rutherford backscattering for the analysis of B-C-N coatings deposited on silicon substrates by Plasma Assisted Chemical Vapor Deposition (PACVD) within the FUNINCOAT network<sup>(1)</sup>. The analysing energy of the  $^4\text{He}$  beam had to be optimised in order to resolve the interfering ( $\alpha,p$ ) reactions on the silicon of the substrate and on the nitrogen of the coating. The signatures of boron and nitrogen and the clean separated silicon background in the NRA detector at a scattering angle of  $\theta_{\text{lab}}=135^\circ$  from the bombardment of a selected B-C-N/Si sample with a 4157 keV  $^4\text{He}$  beam are shown in Fig. 31. For a simple background

---

\* EC Fellow from the University of Strasbourg, France

\*\* EC Fellow from University of Lund, Sweden

<sup>(1)</sup> IRMM Annual Report 95, EUR 16381 EN

identification a blank silicon sample was irradiated under the same conditions and gave the spectrum in Fig. 32.

The simultaneous measured carbon signature in the BS detector at a scattering angle of  $\theta_{lab}=165^\circ$  is a peak sitting on a flat region of the  $(\alpha,\alpha)$  backscattering spectrum of silicon as can be seen in Fig. 33a. The flat nature of the  $(\alpha,\alpha)$  backscattering of silicon in the low energy range of the carbon signature and the non-RBS form at the high energy region obtained with a blank silicon sample are shown (unscaled) in Fig. 33b. The edge energy-shift  $\Delta E_s$  was used for the determination of the energy loss  $\Delta E_c$  in the coating needed for the evaluation of the cross section integrals<sup>(1)</sup>. An expanded view of the carbon signal region together with the separately (unscaled) plotted flat silicon background is presented in Fig. 34.

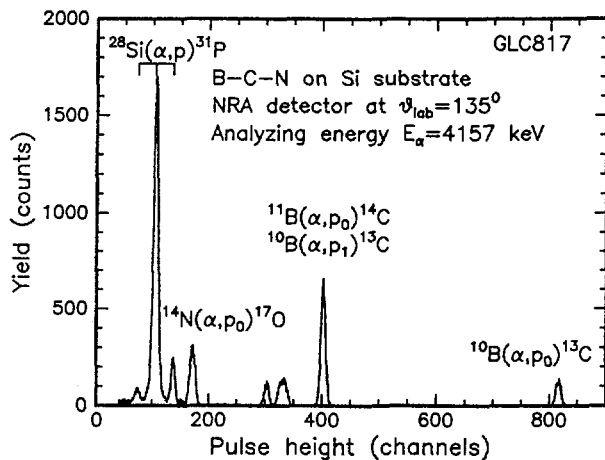


**Fig. 31.** Proton energy spectrum from the irradiation of a B-C-N/Si sample showing the boron and nitrogen signals and the well resolved background from the silicon substrate.

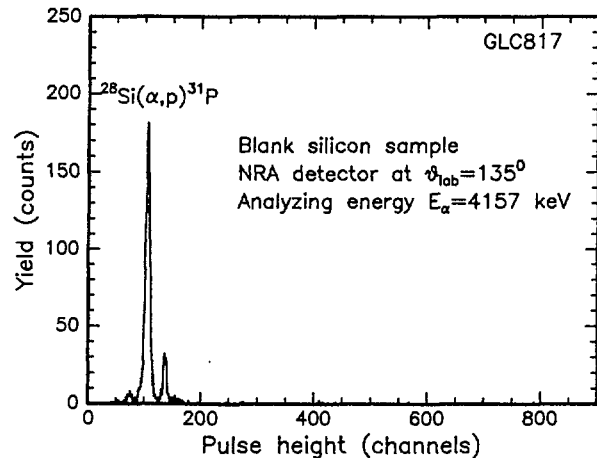


**Fig. 32.** Proton energy spectrum from the irradiation of a blank silicon sample used for a simple background identification.

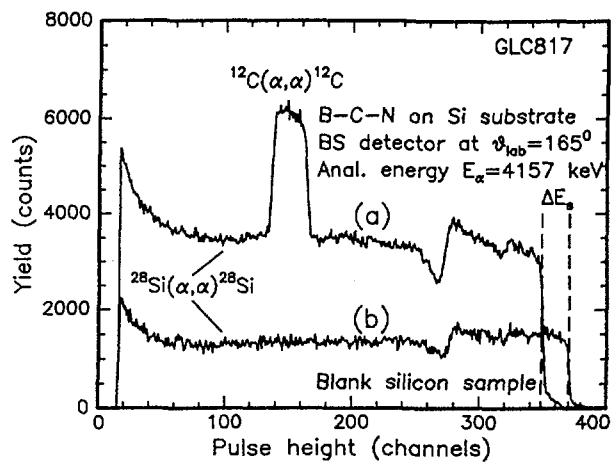


**Fig. 33.** Alpha-particle energy spectra from the irradiation of a B-C-N/Si sample showing the carbon signal (a) and from the bombardment of a blank Si sample plotted separately (unscaled) (b).

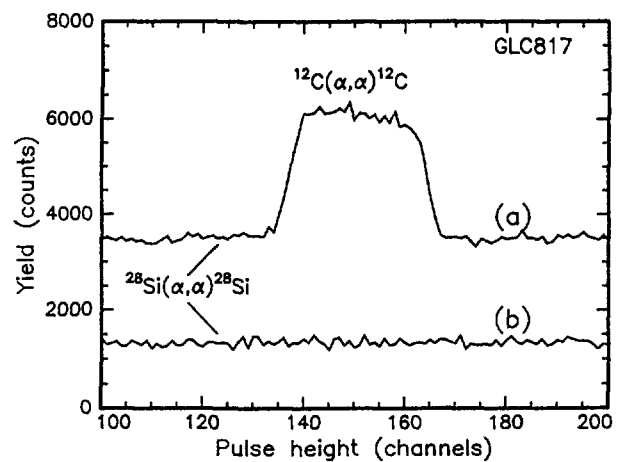


**Fig. 34.** Expanded view of Fig. 33 showing the flat nature of the silicon background in the region of the carbon signal.

The elemental composition of the B-C-N coatings were deduced from the concentration ratios B/C and N/C derived from the measured reaction yields and cross section integrals<sup>(1)</sup> as well as the solid angle ratio between the NRA and BS detectors simply determined with an  $\alpha$ -particle source. The composition obtained from the PCPAA analysis of the selected sample was  $\text{B}_{13.6}\text{C}_{80.1}\text{N}_{6.3}$ . The technique is being currently optimised for the analysis of B-C and C-N films on  $\text{AlSi}_7\text{Mg}$ , a substrate material with excellent mechanical properties for machining and better coating adhesion. However, it is a source of background from the  $(\alpha, p)$  reactions on silicon, aluminium and magnesium.

#### **Hydrogen profiling in B-C-N and B-C thin films**

G. Giorginis, A. Crametz, V. Garcia, M. Hult\*, L. Persson\*

The hydrogen incorporation in boron-carbon nitride (B-C-N) and boron carbide (B-C) coatings on silicon and  $\text{AlSi}_7\text{Mg}$  substrates respectively produced by different deposition techniques within the FUNINCOAT network<sup>(1)</sup> was investigated with the analytical

\* EC Fellow from University of Lund, Sweden

<sup>(1)</sup> IRMM Annual Report 95, EUR 16381 EN

techniques at the 7 MV Van de Graaff accelerator of IRMM. The hydrogen loss was negligible in all samples using  $^4\text{He}$ -ERDA but it was quite high in the B-C-N samples using  $^{15}\text{N}$ -NRRA. This behaviour was studied by measuring the hydrogen concentration as function of the beam dose at the same target point (decay curve) and is demonstrated in Fig. 35 for a selected sample deposited on a silicon substrate by PACVD. The error bars at lower beam dose values are due to shorter irradiations at the beginning of the measurement in order to record the steeply falling part of the decay curve. The dependence of the profile shape on the hydrogen loss was eliminated by first measuring for each sample the decay curve till a quite constant concentration value was reached (asymptotic region) and then starting the profile measurement. The hydrogen depth profile of the selected sample obtained in this way revealed a nearly homogeneous H-distribution inside the coating and the a typical surface contamination peak as shown in Fig. 36.

A surprising and very important finding was the insensitivity of hydrogen to  $^{15}\text{N}$ -beam irradiation in B-C samples as can be seen from the decay curve (Fig. 37) of a sample grown by the technique of Physical Vapor Deposition-Magnetic Sputtering Ion Plating on an  $\text{AlSi}_7\text{Mg}$  substrate with the admixture of 2%  $\text{CH}_4$  gas during deposition (H-enrichment). The corresponding hydrogen depth profile is shown in Fig. 38a together with the profile of a sample grown under the same conditions but without a  $\text{CH}_4$  gas admixture (Fig. 38b). Only the first 120 nm of the 1500 nm thick sample could be profiled due to the maximum attainable energy of approximately 6.6 MeV using the presently available single charged  $^{15}\text{N}$  ions.

B-C samples are potential candidates as hydrogen standards for Ion Beam Analysis (IBA) using normally amorphous silicon (a-Si) standards. The beam resistivity (decay curve) and H-profile of an a-Si standard used at IRMM are presented in Fig. 39 and Fig. 40.

The hydrogen concentration in the B-C film has a homogeneous distribution while in the H-implanted a-Si sample has a Gaussian form. A standard with a homogeneous hydrogen distribution simplifies the calibration procedures and there is a need for it in IBA work. Discussions about the development and characterisation of B-C hydrogen standards have been started between IRMM and the FUNINCOAT partner producing the investigated B-C coatings. In order to obtain quantitative H-concentration values for the B-C-N samples with the  $^{15}\text{N}$ -NRRA technique the decay curves have to be measured with higher precision and a proper function has to be fitted for the determination of the zero-dose

concentration. Presently the complementary technique of  $^4\text{He}$ -ERDA is used for quantitative work before applying  $^{15}\text{N}$ -NRRA for the measurement of the profile shape.

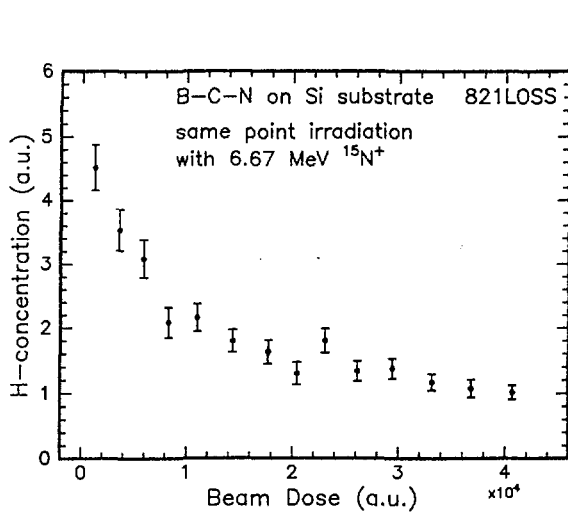


**Fig. 35.** Hydrogen concentration versus beam dose (decay curve) of a B-C-N coating on a Si substrate irradiated by 6.67 MeV  $^{15}\text{N}^+$  ions at the same point.

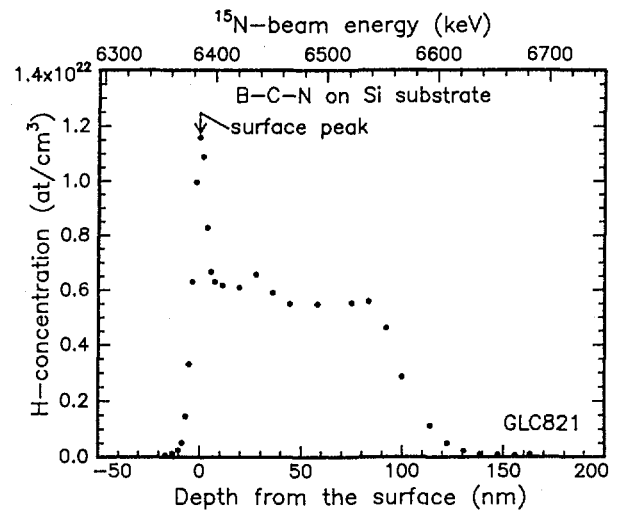


**Fig. 36.** Hydrogen distribution in the B-C-N sample used to produce Fig. 56. Depth profiling by  $^{15}\text{N}$ -NRRA was performed in the asymptotic region of the decay curve.

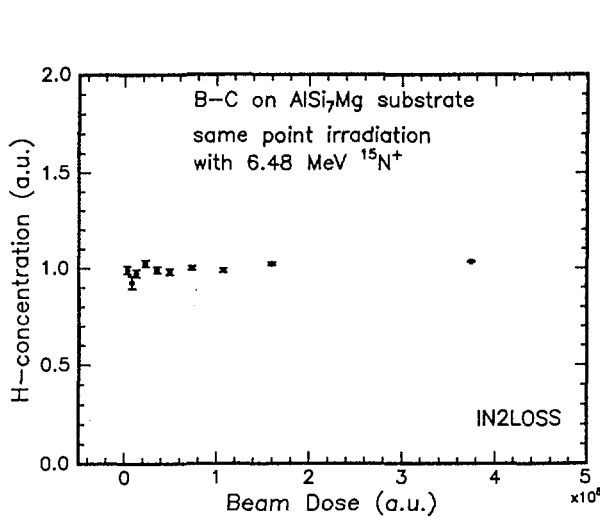


**Fig. 37.** Hydrogen decay curve of a B-C coating on a AlSi<sub>7</sub>Mg substrate irradiated by 6.48 MeV  $^{15}\text{N}^+$  ions.

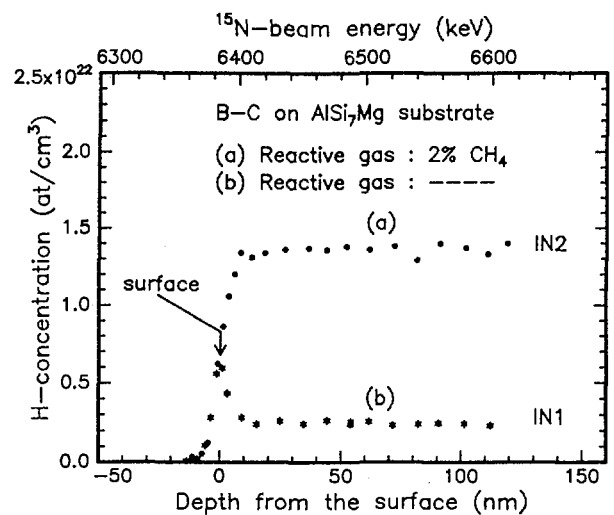


**Fig. 38.** Hydrogen depth profile measured by  $^{15}\text{N}$ -NRRA: (a) in the hydrogen enriched B-C sample used to produce Fig. 37 and (b) in a sample from the same production without hydrogen enrichment (intrinsic hydrogen).

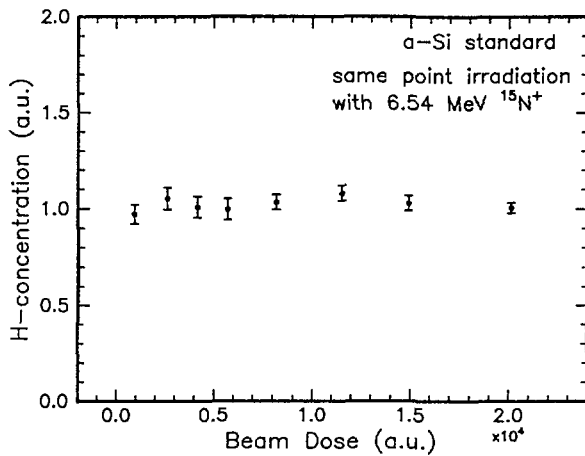


**Fig. 39.** Hydrogen decay curve of a 10 keV  $H^+$  implanted a-Si standard irradiated by 6.54 MeV  $^{15}N^+$  ions.

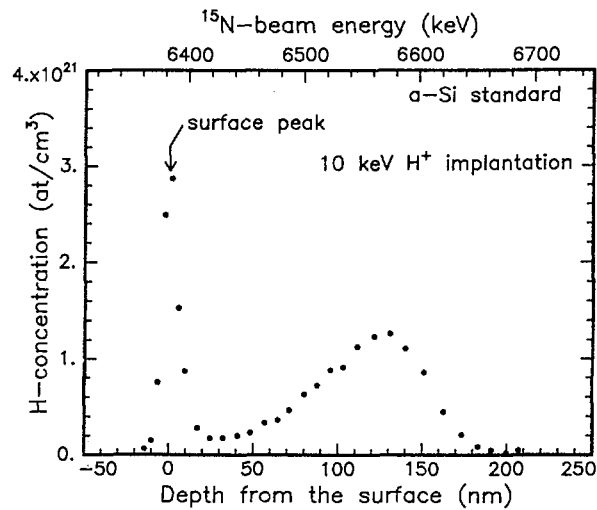


**Fig. 40.** Hydrogen depth profile measured by  $^{15}N$ -NRRA in the a-Si standard used to produce Fig. 39.

### *Development and Operation of the IRMM Networks*

H. Horstmann, C. Bastian, C. Cervini, T. Garcia, G. Kelly

The existing Scientific Network of IRMM was operated, maintained and continuously monitored. A significant increase in data transfer within and between the buildings made an improvement of performance necessary. Accordingly switching equipment was introduced to provide a segmentation of the network, thus avoiding unnecessary traffic between the buildings.

A second network -physically distinct from and not connected to the scientific network - was specified and installed as part of the Joint Research Centre Corporate Network. The purpose of the Corporate Network is to connect all administrative services of the JRC in a single, protected Intranet. In Geel, it physically consists of twisted pair cabling of several administrative users' offices in a star arrangement around a central hub in the main building. A fibre link connects this hub to a second one in the Linac building where the connection to the other JRC establishments is done via a router and a modem. The systems connected in Geel to the Corporate network are one server running Windows NT and several workstations running Windows 95. They use TCP/IP as the main network protocol.

Since September 96, the Scientific network has a 128kB connection to Internet, as provided by the Belgian research network BELNET. The Internet domain name is **irmm.jrc.be**. The essential network servers, i.e. the Domain Name Server, the gateway

control, the mail server and an intranet server are hosted in two RS/6000 systems. The mail server handles both SMTP and X400 protocols. The Intranet server provides access to a repository of template documents and common applications, which may be downloaded as required into any users' PC connected to the network.

### ***Support to PC Users***

T. Garcia, C. Nazareth, D. De Pooter, P. Van Roy, L. Van Rhee

Like in all other establishment of the JRC, the Rank Xerox Office automation systems used by the secretaries were phased out and replaced by networked personal computers. Concurrently, an important demand of equipment from all units in the institute resulted in installation of 73 Pentium PC's and 20 Printers. All new PC's installed run the MS Windows for Workgroups or Windows 95 as standard operating systems. Basing on a contract with Siemens/Microsoft, the INF Unit also equips these PC's with desktop products in the Microsoft Office Suite (e.g. MS Word and Excel in standard).

All new PC's connected to the scientific network or to the JRC Corporate Network use TCP/IP as a standard communication protocol. Other network protocols such as XNS are being discarded. On user's request, PC's with authorised access to Internet are equipped with a network browser, either Netscape or MS Explorer.

For electronic mail, secretariat PC's are equipped with the product ISOPRO to conform to the Commission X400 mail standard. Freeware products like EUDORA-light and PINE are implemented on the other PC's running SMTP mail. Conversion tables in the gateway of the mail server allow these two mail systems to communicate with each other.

The Samba software suite has been added to several UNIX systems, in order to integrate their resources (disks and printers) more easily in MS Windows LAN.

### ***Design and Production of Special Electronic Instrumentation***

S. de Jonge, J. Gonzalez, K. Hofmans, H. Mensch, H. Nerb

An opto coupled scaler interface has been developed. The unit is a PC board, which can be built into an existing interface providing opto coupling at output, ready and start/stop levels.

For multiparameter acquisition measurements a Modular Multiparameter Multiplexer (M.M.P.M.) has been designed and constructed as a double NIM unit. The multiplexer has four 16 bit inputs and one 16 bit output. The four input channels are buffered with a

1K FIFO and have a dead time of 0,3 $\mu$ s. The units can be cascaded and might operate in free or coincidence mode. The maximum throughput is 2.106 bytes/sec.

To monitor the radiation diagram of the LINAC target a Monitor Ratio Converter was developed. The single NIM converter can measure the count rate ratio of two neutron monitors and is generating a DC output from 0 tot 10V with a resolution of 10 bits. The maximum ratio range is 16.

A Delaying T0- Gate has been designed, with the purpose of preventing Time-Of-Flight measurements during the unstabilised start up period of the LINAC. It blocks the T0 signal during the first 5 minutes of its appearance.

The introduction of the fast Canberra 8715 ADC led to the design of an ADC interface to the 3 parameter PC based acquisition system (MULIM).

## LIST OF PUBLICATIONS

### CONTRIBUTIONS TO CONFERENCES

BASTIAN C.

AGS, a set of UNIX commands for neutron data reduction  
5th Int. Conf. on Applications of Nuclear Techniques, Crete, June 9-15, 1996

BEER, H., MUTTI, P., CORVI, F., MOHR, P., OBERHUMMER, H.

Neutron capture reactions in s- and r-process nucleosynthesis  
9th International Symposium on Capture Gamma Ray Spectroscopy and related topics,  
Budapest, 8-12 October 1996

BIEBER, R., WAGEMANS, C., HEYSE, J., BALCAEN, N., BARTHELEMY, R., VAN GILS, J.

Measurement of the  $^{36}\text{Cl}(n, \alpha)^{33}\text{P}$  reaction cross-sections as a function of the neutron energy

9th International Symposium on Capture Gamma Ray Spectroscopy and related topics,  
Budapest, 8-12 October 1996

BIRN, I.G., WATTECAMPS, E.

Measurement of inelastic neutron scattering cross sections for low lying levels of  $^{92}\text{Mo}$  and  $^{10}\text{Mo}$

Frühjahrstagung der Deutschen Physikalischen Gesellschaft, Stuttgart, 25-29 March, 1996

CORVI, F., ATHANASSOPOULOS, K., BEER, H., MUTTI, P., POSTMA, H., ZANINI, L.

Resonance neutron capture studies

14th International Conf. on the application of accelerators in research and industry,  
Denton, USA, 6-9 November 1996

CORVI, F., MUTTI, P., ATHANASSOPOULOS, K., BEER, H.

The stellar capture rate of  $^{136}\text{Ba}$

Nuclei in the Cosmos IV 1996, Notre Dame, June 20-27, 1996

DEMATTE, L., WAGEMANS, C., D'HONDT, P., BARTHELEMY, R., DERUYTTER, A.J.

Characteristics of the spontaneous fission decay of even-even plutonium isotopes

Internat. Symposium on Large Scale Collective Motion of Atomic Nuclei, Boro, October 15-19, 1996

GODDIO, C., WATTECAMPS, E.

Feasibility test of neutron inelastic cross section measurements by the time of flight technique

Frühjahrstagung der Deutschen Physikalischen Gesellschaft, Stuttgart, March 25-29, 1996

HAMBSCH, F.-J., BAX, H., OBERSTEDT, S., VIVES, F.

Neutron induced fission of  $^{238}\text{U}$  at incident neutron energies between 1.6 and 4.0 MeV

Int. Symposium on Large Scale Collective Motion on Atomic Nuclei, Brolo, 15-19 October 1996

HAMBSCH, F.-J., OBERSTEDT, S., VAN AARLE, J.

$^{252}\text{Cf}(sf)$ , still interesting?

North-West Europe Nuclear Physics Conference, Amsterdam, April 16-19, 1996

MEISTER, A., WATTECAMPS, E., KONING, A.J., HOGENBIRK, A., GRUPPELAAR, H.

Cross sections of inelastic neutron scattering from palladium isotope nuclei  
Frühjahrstagung der Deutschen Physikalischen Gesellschaft, Stuttgart, 25-29 March 1996

OBERSTEDT, S., HAMBSCH, F.-J., VIVES, F.

The multi-modal random neck-rupture model - revision and application  
Int. Symposium on Large Scale Collective Motion on Atomic Nuclei, Brolo, 15-19 October, 1996

OBERSTEDT, S., HAMBSCH, F.-J., VIVES, F.

Study of fission fragment properties of  $^{239}\text{U}$   
Frühjahrstagung der Deutschen Physikalischen Gesellschaft, Stuttgart, 25-29 March 1996

PERSSON, L., HULT, M., GIORGINIS, G., CRAMETZ, A.

Hydrogen depth profiling at IRMM  
14th Int. Conf. on the Application of Accelerators in Research and Industry, Denton, 6-9 November 1996

WAGEMANS, C., LOISELET, M., BIEBER, R., DENECKE, B., REHER, D.F.G., GELTENBORT, P.

Preparation, Characterisation and testing of implanted  $^{37}\text{Ar}$  layers  
18th World Conference on the INTDS, Strasbourg, 7-11 October 1996

ZANINI, L., CORVI, F., ATHANASSOPOULOS, K., POSTMA, H., GUNSING, F.

Spin assignment of  $^{109}\text{Ag}$  neutron resonances  
9th International Symposium on Capture Gamma Ray Spectroscopy and related topics, Budapest, 8-12 October 1996

## SCIENTIFIC OR TECHNICAL ARTICLES

### *PUBLISHED*

BASTIAN, C.

Real-time multiparametric analysis in a single processor  
IEEE Trans. Nucl. Sci. 43(1996)2343

COCEVA, C., BRUSEGAN, A., VAN DER VORST, C.

Gamma intensity standard from thermal neutron capture in  $^{35}\text{Cl}$   
Nucl. Instr. and Meth. A378(1996)511

GIORGINIS, G.

Prompt charged particle activation analysis for light elements determination  
Nucl. Instr. and Meth. B118(1996)172

GIORGINIS, G., MISAEELIDES, P., CRAMETZ, A., CONTI, M.

Cross section of the  $^{14}\text{N}(\alpha, p_0)^{17}\text{O}$  nuclear reaction for analytical applications  
Nucl. Instr. and Meth. B 113(1996)396

GIORGINIS, G., MISAEELIDES, P., CRAMETZ, A., CONTI, M.

Cross section of the  $\text{B}(\alpha, p)\text{C}$  nuclear reaction for analytical applications  
Nucl. Instr. and Meth. B118(1996)224

MOUCHEL, D., WORDEL, R.

A low-energy HPGe detector dedicated to radioactivity measurements far below environmental levels

Appl. Radiat. Isot. 47(1996)1033

NOLI, F., MISAEALIDES, P., GIORGINIS, G., BAUMANN, H., HAUSNER, R.

Application of the nuclear analytical and electron microscopic techniques to the investigation of the oxidation behaviour of Mg-implanted steel samples

Nucl. Instrum. and Methods Phys. Res. B131(1996)171

POSTMA, H., GUNSING, F., CORVI, F.

Improved analysis of parity violation at neutron p-wave resonances of U-238 based on resonance spin assignments

Phys. Review C55(1996)R558

QUINTANA, B., FERNANDEZ, F., WORDEL, R., MOUCHEL, D.

Automatic analysis of continuum phenomena in gamma spectra

Appl. Radiat. Isot. 47(1996)911

REHER, D.F.G.

Metrology of  $^{192}\text{Ir}$  brachytherapy sources, EUROMET Project Nr. 219-Part A: Air Kerma Rate Measurements

Metrologia 32(1996)405

REHER, D.F.G.

Metrology of  $^{192}\text{Ir}$  brachytherapy sources, EUROMET Project Nr. 219-Part B: Activity Measurements

Metrologia 32(1996)407

SVIRIN, M.I., SMIRENKIN, G.N., HAMBSCH, F.-J.

Spectra of fission neutrons and nuclear level density (testing of the generalised superfluid model)

Physics of Atomic Nuclei 59(1996)965

VAN 'T HOF, G, BACELAR, J.C., DIOSZEGI, I., HARAKEH, M.N., HESSELINK, U.H.A., KALANTAR-NAYESTANAKI, N., KUGLER, A., VAN DER PLOEG, H., PLOMPEN, A.J.M., VAN SCHAGEN, J.P.S.

Viscosity and fission time scale of  $^{156}\text{Dy}$

Phys. Rev. C54(1996)R1515

WAGEMANS, C., BIEBER, R., GELTENBORT, P.

Determination of the  $^{36}\text{Cl}(n_{\text{th}},p)$  and  $^{36}\text{Cl}(n_{\text{th}},a)^{33}\text{P}$  reaction cross-sections: Part 1: measurements with thermal neutrons

Phys. Review C54(1996)389

WAGEMANS, C., DEMATTE, L., POMME, S., SCHILLEBEECKX, P.

Mass and energy distributions for  $^{243}\text{Am}(n_{\text{th}},f)$

Nuclear Physics A597(1996)188

WORDEL, R., MOUCHEL, D., ALTZITZOGLOU, T., HEUSSER, G., QUINTANA ARNES, B., MEYNENDONCKX, P.

Study of neutron and muon background in low-level germanium gamma-ray spectrometry

Nucl. Instrum. Methods Phys. Res. A369(1996)557

WORDEL, R., MOUCHEL, D., STEINBAUER, E., OYRER, R.

An active background discrimination technique using a multiple detector event by event recording system

Appl. Radiat. Isot. 47(1996)1061

*IN PRESS*

BEER, H., CORVI, F., MUTTI, P.

Neutron capture of the bottle-neck isotopes  $^{138}\text{Ba}$  and  $^{208}\text{Pb}$ , s-process studies and the r-process abundance distribution

The Astrophysical Journal

DEMATTE; L., WAGEMANS, C., BARTHELEMY, R., D'HONDT, P., DERUYTTER, A.

Fragments' mass and energy characteristics in the spontaneous fission of  $^{236}\text{Pu}$ ,  $^{238}\text{Pu}$ ,  $^{242}\text{Pu}$  and  $^{244}\text{Pu}$

Nucl. Phys. A.

HAMBSCH, F.-J., OBERSTEDT, S.

Investigation of the far asymmetric region in  $^{252}\text{Cf}(\text{sf})$

Nuclear Physics A

HOOGWERF, J.A., VAN BERGEN, M.J., HERTOGEN, J., VROON, P.Z., WORDEL, R., SNEYERS, A., NASUTION, A., MOENS, H.L.E., MOUCHEL, D.

Systematic behaviour of U, Th and Ra isotopes across an active island arc-continent collision zone

Geochimica et Cosmochimica Acta

MUTTI, P., CORVI, F., ATHANASSOPOULOS, K., BEER, H.

The stellar capture rate of  $^{136}\text{Ba}$

Nucl. Phys. A

OBERSTEDT, S., HAMBSCH, F.-J.

Assessment of shape isomeric half-lives in the light actinide region

Nucl. Phys. A

TSABARIS, C., WATTECAMPS, E., ROLLIN, G., PAPADOPOULOS, C.T.

Measured and calculated differential and total yield cross section data of  $^{58}\text{Ni}(n,x\alpha)$  and  $^{63}\text{Cu}(n,xp)$  in the neutron energy range from 2.0 to 15.6 MeV

Nucl. Sci. Eng.

*SPECIAL PUBLICATIONS*

HANSEN, H.H. (ed.)

Annual Report 95. Institute for Reference Materials and Measurements

EUR 16381 EN

HANSEN, H.H. (ed.)

Annual Progress Report on Nuclear Data 1995

EUR 16417 EN

**GLOSSARY**

ANL	Argonne National Laboratory, Argonne (USA)
BIPM	Bureau International des Poids et Mesures, Sèvres (F)
CCMRI	Comité Consultatif pour les Etalons de Mesures des Rayonnements Ionisants
CEA	Commissariat à l'Energie Atomique, Paris (F)
CIPM	Comité International des Poids et Mesures
CPAA	Charged Particle Activation Analysis
CNRS	Centre National de la Recherche Scientifique
DAMRI	Departement des Applications et de la Métrologie des Rayonnements Ionisants
DG	Direction Générale
EFF	European Fusion File
ENDF	Evaluated Nuclear Data File
ERDA	Elastic Recoil Detection Analysis
ETL	Electrotechnical Laboratory, Ibaraki (Japan)
EU	European Union
FP	Flight Path
FWHM	Full Width at Half Maximum
GELINA	Geel Electron Linear Accelerator
HPGe	High Purity Germanium
IAEA	International Atomic Energy Agency, Vienna (A)
IBA	Ion Beam Analysis
ICRM	International Committee for Radionuclide Metrology
ILL	Institut Laue-Langevin, Grenoble (F)
INDC	International Nuclear Data Committee
IRMM	Institute for Reference Materials and Measurements, Geel (B)
JEF	Joint European File
JRC	Joint Research Centre
KFA	Kernforschungsanlage, now : Forschungszentrum, Jülich (D)
KFK	Kernforschungszentrum Karlsruhe, now: Forschungszentrum, Karlsruhe (D)

LANL	Los Alamos National Laboratory (USA)
LPRI	Laboratoire Primaire des Rayonnements Ionisants (F)
LSC	Liquid Scintillation Counting
NAA	Neutron Activation Analysis
NEA	Nuclear Energy Agency, Paris (F)
NEANDC	Nuclear Energy Agency's Nuclear Data Committee
NIST	National Institute of Standards and Technology, Gaithersburg (USA)
NMI	Nederlands Meetinstituut, Bilthoven (NL)
NPL	National Physical Laboratory, Teddington (UK)
NRA	Nuclear Reaction Analysis
NRRA	Nuclear Resonant Reaction Analysis
OMH	Országos Mérénygi Hivatal, Budapest (H)
ORELA	Oak Ridge Electron Linear Accelerator
OTR	Optical Transition Radiation
PCPAA	Prompt Charged Particle Activation Analysis
PNC	Parity Non Conservation
PSD	Pulse Shape Discrimination
PTB	Physikalisch-Technische Bundesanstalt, Braunschweig (D)
RPL	Radiation Physics Laboratory
RUG	Rijksuniversiteit Gent, now : Universiteit Gent (B)
SCK/CEN	Studiecentrum voor Kernenergie/ Centre d'Etudes Nucléaires, Mol (B)
SI	Système International d'Unité
SIR	Système International de Référence
TH	Technische Hochschule
TOF	Time of Flight
TR	Transition Radiation
TU	Technical University
TUI	Transuranium Institute (JRC Karlsruhe)
VITO	Vlaamse Instelling voor Technologisch Onderzoek, Mol (B)
WREND A	World Request List for Neutron Data Measurements

## CINDA ENTRIES LIST

ELEMENT		QTY	TYPE	ENERGY		DOCUMENTATION		LAB	COMMENTS
S	A			MIN	MAX	REF VOL PAGE	DATE		
U	238	NF	EXP	16+4	35+4	INDC(EUR) 031-16	97	GEL	VIVES HAMBSCH TKE VALUES.
Pu	236	SF	EXP			INDC(EUR) 031-21	97	GEL	WAGEMANS - SF/ PU239 NF
Pu	238	SF	EXP			INDC(EUR) 031-21	97	GEL	WAGEMANS - SF/ PU239 NF
Pu	240	SF	EXP			INDC(EUR) 031-21	97	GEL	WAGEMANS - SF/ PU239 NF
Pu	242	SF	EXP			INDC(EUR) 031-21	97	GEL	WAGEMANS - SF/ PU239 NF
Pu	244	SF	EXP			INDC(EUR) 031-21	97	GEL	WAGEMANS - SF/ PU239 NF
Pu	239	SF	EXP			INDC(EUR) 031-21	97	GEL	WAGEMANS - NF THERMAL
Ag	109	NG	EXP	30+0	12+2	INDC(EUR) 031-38	97	GEL	CORVI - SPIN ASSIGNMENT
Na	23	NNG	EXP	44+4	20+5	INDC(EUR) 031-25	97	GEL	KOPECKY Res Analysis
Al	27	NNG	EXP	44+4	20+5	INDC(EUR) 031-25	97	GEL	KOPECKY Res Analysis.
Fe	56	NNG	EXP	44+4	30+5	INDC(EUR) 031-25	97	GEL	DUPONT Res Analysis.
B	10	NT	EXP	40+4	19+5	INDC(EUR) 031-26	97	GEL	CRAMETZ PLOMPEN Dev ENDF.
O	17	NA	EXP	25-3	25-3	INDC(EUR) 031-27	97	GEL	WAGEMANS NUCLEOSYNTH.
Ar	37	NA	EXP	10+1	10+4	INDC(EUR) 031-29	97	GEL	BIEBER NUCLEOSYNTH. S36
Ba	136	NG	EXP	60+3	20+4	INDC(EUR) 031-30	97	GEL	MUTTI, CORVI BEER.
Tc	99	NT	EXP	10+2	10+4	INDC(EUR) 031-31	97	GEL	BRUSEGAN GUNSING LEPRETRE
Tc	99	NG	EXP	10+2	10+4	INDC(EUR) 031-31	97	GEL	CORVI RAEPSAET LEPRETRE
Mo	90	NNG	EXP	55+5	55+5	INDC(EUR) 031-32	97	GEL	WEIGMANN - BIRN EXCIT. FUNCT.
U	238	NN	EXP	20+5	35+5	INDC(EUR) 031-36	97	GEL	GODDIO PLOMPEN
Fe	54	NXN	EXP	20+4	20+6	INDC(EUR) 031-41	97	GEL	FESSLER QUAIM ISOM. XSECT
Ni	58	NX	EXP	16+6	20+6	INDC(EUR) 031-43	97	GEL	WATTECAMPS - ACTIVATION
Pb	208	NNG	EXP	14+4	30+5	INDC(EUR) 031-37	97	GEL	KOPECKY INELASTIC

European Communities - Commission

EUR 17687 EN, ANNUAL PROGRESS REPORT ON NUCLEAR DATA 1996

Institute for Reference Materials and Measurements

H. H. Hansen (ed.)

Luxembourg: Office for Official Publications of the European Communities

1997 - PAG. 73- 21.0 x 29.7 cm

EN

## NOTICE TO THE READER

All scientific and technical reports published by the European Commission are announced in the monthly periodical '**euro abstracts**'. For subscription (1 year: ECU 60) please write to the address below.



OFFICE FOR OFFICIAL PUBLICATIONS  
OF THE EUROPEAN COMMUNITIES

L-2985 Luxembourg

---